

THE LOCATION AND SOURCE PARAMETERS OF THE LOMPOC, CALIFORNIA, EARTHQUAKE OF 4 NOVEMBER 1927

BY D. V. HELMBERGER, P. G. SOMERVILLE, AND E. GARNERO

ABSTRACT

In this paper, we address the relocation, magnitudes, and the style of faulting of the Lompoc earthquake from a sparse assortment of teleseismic and regional seismograms. The highest quality teleseismic waveform data come from a station at De Bilt (Netherlands) that remains in operation. Thus, recordings of numerous modern events in central coastal California (i.e., the 1969 Santa Lucia Banks, 1983 Coalinga, 1978 Santa Barbara, and 1989 Loma Prieta earthquakes) have been used for comparison with the 1927 records. Location constraints for the Lompoc event were established from the De Bilt recording by comparing *S-P* and *SSS-S* waveform matches against the above master events to avoid the effect of unknown clock errors on locations that use absolute times. These same seismograms were modeled to estimate the depth, faulting parameters, and source strength. A similar approach using observational comparisons and numerical modeling was applied to the regional waveform data obtained from the stations at Berkeley, Tucson, and Pasadena.

Our results indicate a north-northwesterly striking reverse event located about 40 km west of Point Conception, which is in excellent agreement with the recent tsunami modeling results by Satake and Somerville (1992). This location is 25 km south of that proposed by Hanks (1979) and well within his error bars. We obtain a body-wave moment of 1×10^{26} dyne-cm, a trapezoidal time history of (2, 2, 2) sec. and a source depth of 10 km. The weak beginning of the *Pnl* wavetrain at Berkeley indicates some source complexity, which is characteristic of many large events. The fault parameters are strike = N20°W, dip = 66°NE, and rake = 95°. Most seismicity catalogs report a $M_s = 7.3$ for this event, after Gutenberg and Richter (1956), but this was a long-period body-wave magnitude and not a surface-wave result. Their original worksheets indicate a smaller $M_s = 7.0$. The body waves of the Loma Prieta event ($M_s = 7.1$) appear distinctly larger than those of the Lompoc event at De Bilt, in agreement with our lower estimate of source strength.

INTRODUCTION

The 1927 Lompoc earthquake (4 November 0551 Pacific Standard Time, $M_s = 7.0$) occurred before the deployment of regional seismic arrays in California, with the result that the location and mechanism of the earthquake have been subject to considerable uncertainty. Byerly (1930) used regional travel-time data to locate the event offshore Point Arguello at 34.5°N, 121.4°W (Fig. 1). Gawthrop (1978, 1981) located it at 34.9°N 120.7°W, much closer to the coast near Point Sal, using teleseismic travel-time data, and suggested that this earthquake occurred on the Hosgri fault. Hanks *et al.* (1975) and Hanks (1979, 1981) located it at an intermediate position of 34.6°N, 120.9°W using regional seismic data from the mainshock and aftershocks. This uncertainty in location has resulted in uncertainty in the tectonic interpretation of the event and its association with active offshore faults. However, the development of synthetic seismogram techniques in recent years in conjunction with a set of recent earthquakes has provided an opportunity to obtain more accurate estimates of

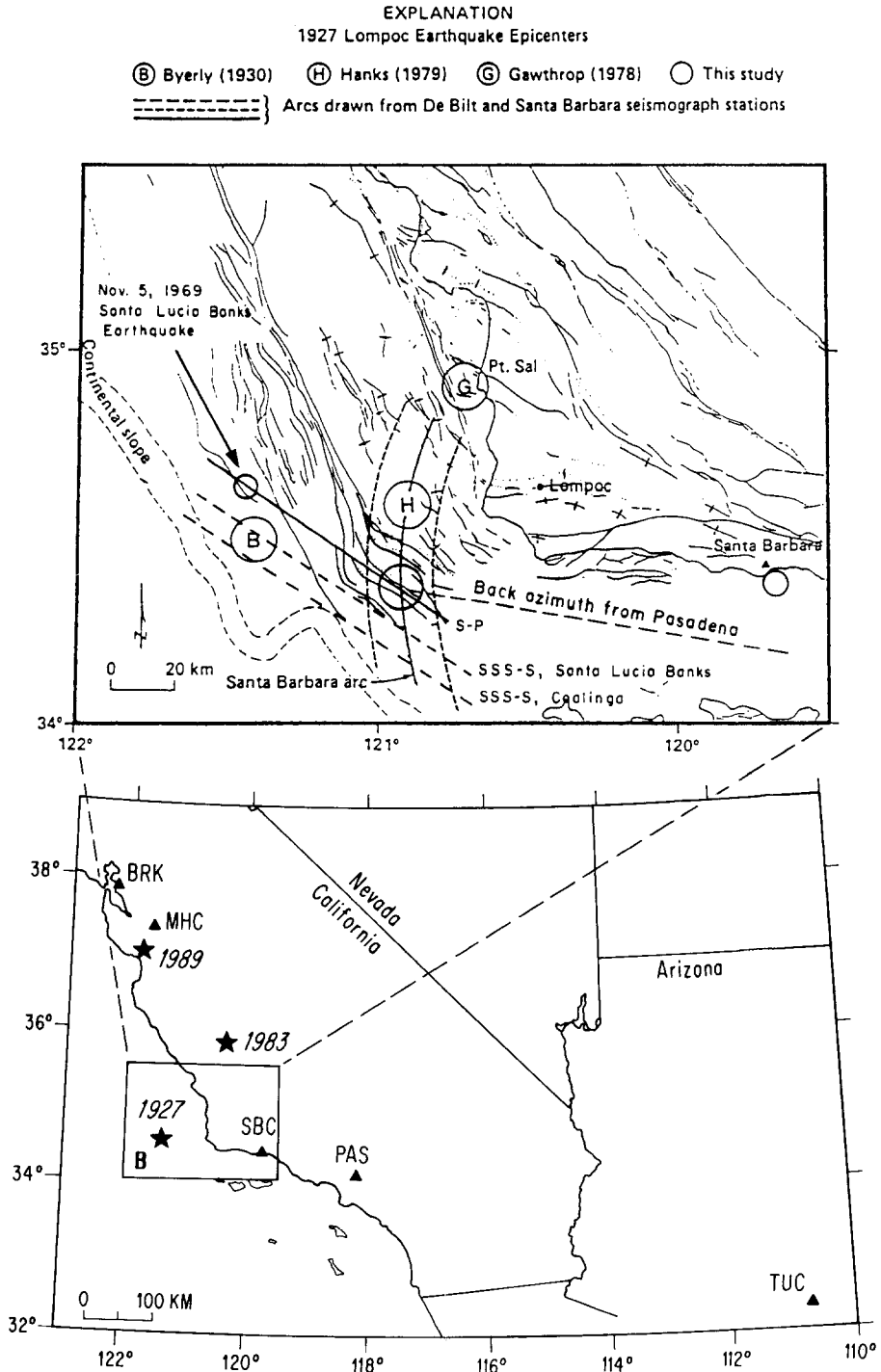


FIG. 1. Constraints on the location of the 1927 Lompoc earthquake from differential travel times of *P*, *S* and *SSS* phases at De Bilt with respect to the 1969 Santa Lucia Banks and 1983 Coalinga earthquakes, from *S-P* times of aftershocks recorded at Santa Barbara, and from the backazimuth of *P* waves recorded at Pasadena. *Inset* shows regional map indicating earthquake locations (including Byerly's location of the 1927 event) and seismic stations.

the location, focal depth, focal mechanism, and seismic moment of the earthquake using the sparse azimuthal distribution of available seismograms.

The regional seismograms for this event have mostly been lost, but fortunately Byerly (1930) published recordings from Berkeley (BKS), Lick, and Tucson (TUC), shown in Figure 2. Included in Figure 2 are Byerly's picks of P and S at BKS used in locating the event by Byerly and later by Hanks (1979). The identification and interpretation of seismic phases on these seismograms is problematical, as pointed out by Gawthrop (1981). The most useful regional recording is the TUC record, since long-period torsion instruments have proven reliable and have been operated for many years at other stations, such as Pasadena. A beginning portion of the Pasadena torsion reading is also available and will be discussed later. The poorest set of observations are clearly from Lick where only the NS component looks reasonable. Note the asymmetric arcs on the EW and Z components. The Bosch-Omori records from the BKS station appear stable and prove useful.

The responses of the instruments used in this study are given in Figure 3 where we have included a small amount of attenuation ($t^* = 0.1$) to stabilize the responses. Included in this figure are the instrumental constants used in their construction. These constants were obtained from Poppe (1980) and Kanamori (1988). There is some uncertainty in the damping coefficients assumed for these instruments, especially in the Weichert systems that generally yield seismograms with strong ringing similar to the NS component of the Lick record; this ringing is not predicted from the response shown in Figure 3.

The stability of the Bosch-Omori seismographs at Berkeley is discussed at length by Bakun and McEvelly (1984). The gain remains somewhat unclear but their calculations for the Parkfield events assumed a gain of 50 for 1922 and 45 for the 1934 event. The difference between the constants derived by their investigations and the response gains in Figure 3 is not significant for our purposes. These authors give an excellent critique of teleseismic seismograms obtained from the other worldwide stations for their Parkfield sequence, pointing out the difficulties in using historic data with ambiguous responses during this era. They conclude that the De Bilt station is by far the most dependable, as has been discovered by many subsequent researchers, (Kanamori 1988). In fact, the only known teleseismic instrument that recorded the Lompoc event and is still in operation is at De Bilt, Netherlands. The Galitzin response is relatively short-period compared with the WWSSN long-period response (Fig. 3), which makes it an excellent instrument for modeling body waves, but less suitable for modeling surface waves. Yeh (1975) used De Bilt in her Lompoc surface-wave study and reported great difficulty in finding a stable solution. She estimated a moment of 4.5×10^{26} dyne-cm for a NE-dipping fault and 8.5×10^{26} dyne-cm for a SE-dipping fault. However, modeling short-period surface waves (15 sec) at teleseismic distances has not gained acceptance by the seismological community, since their crustal propagation introduces large variations in amplitudes. Comparative studies can still be done when a modern event with well-determined parameters calibrates the path, as is discussed later. From the overall comparisons between the Lompoc and the 1989 Loma Prieta seismograms at De Bilt displayed in Figure 4, we conclude that the Lompoc event is smaller than the 1989 Loma Prieta event, whose moment is 3×10^{26} (Kanamori and Satake, 1990). The De Bilt station reports an $M_s = 7.1$ for Loma Prieta and, applying their formula, an $M_s = 7.0$ for Lompoc.

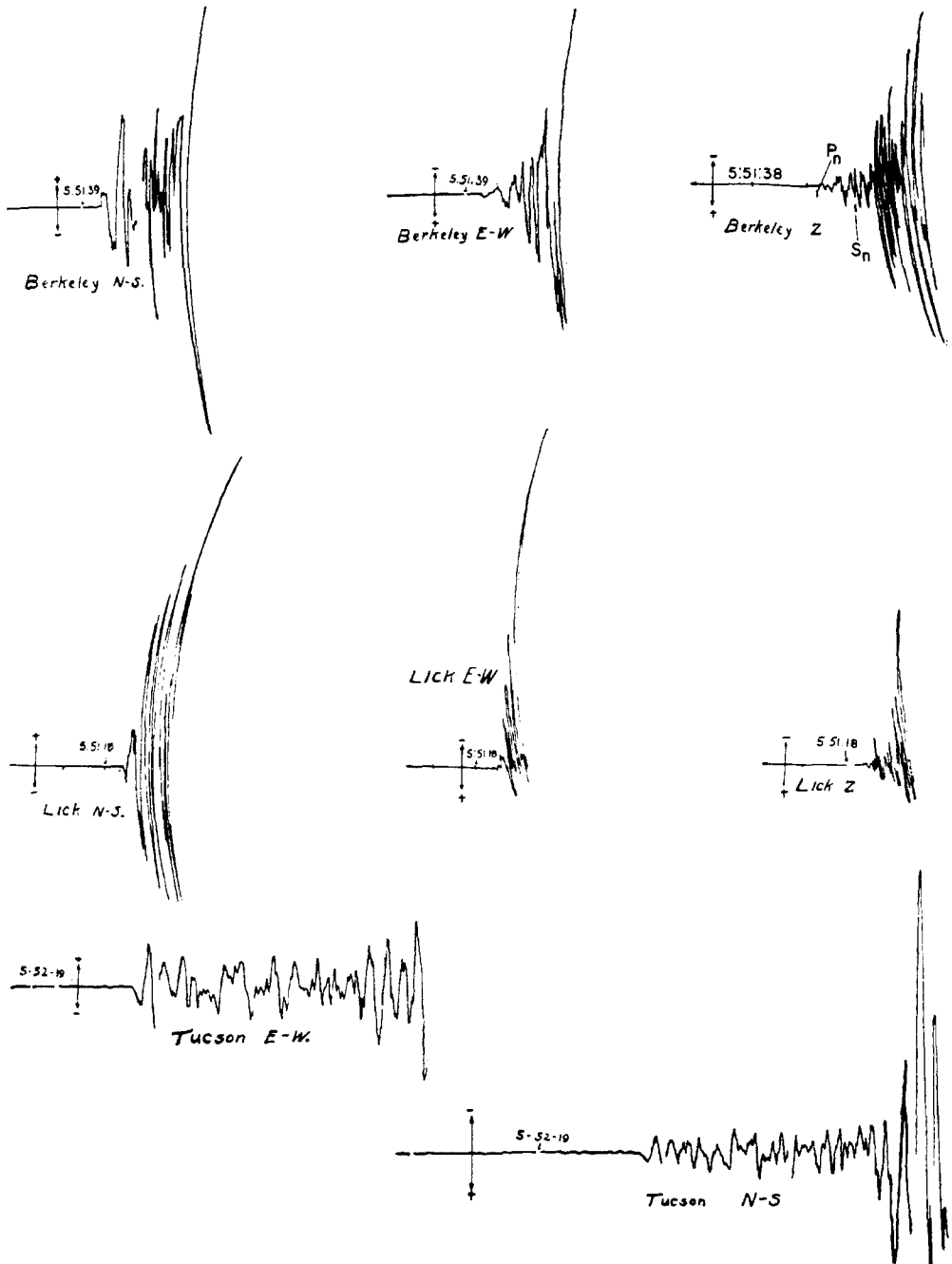


FIG. 2. Display of regional recordings of the 1927 Lompoc earthquake. The distances are roughly 350 km to BKS and 960 km to TUC (Tucson, Arizona). After Byerly (1930). (The Lick station is referred to as MHC on the location map in Figure 1.)

The magnitudes of large earthquakes that occurred in the first half of this century have been the subject of intensive re-evaluation during the past two decades. In particular, Geller and Kanamori (1977) reviewed the procedures used by Gutenberg and Richter in estimating magnitudes and concluded that

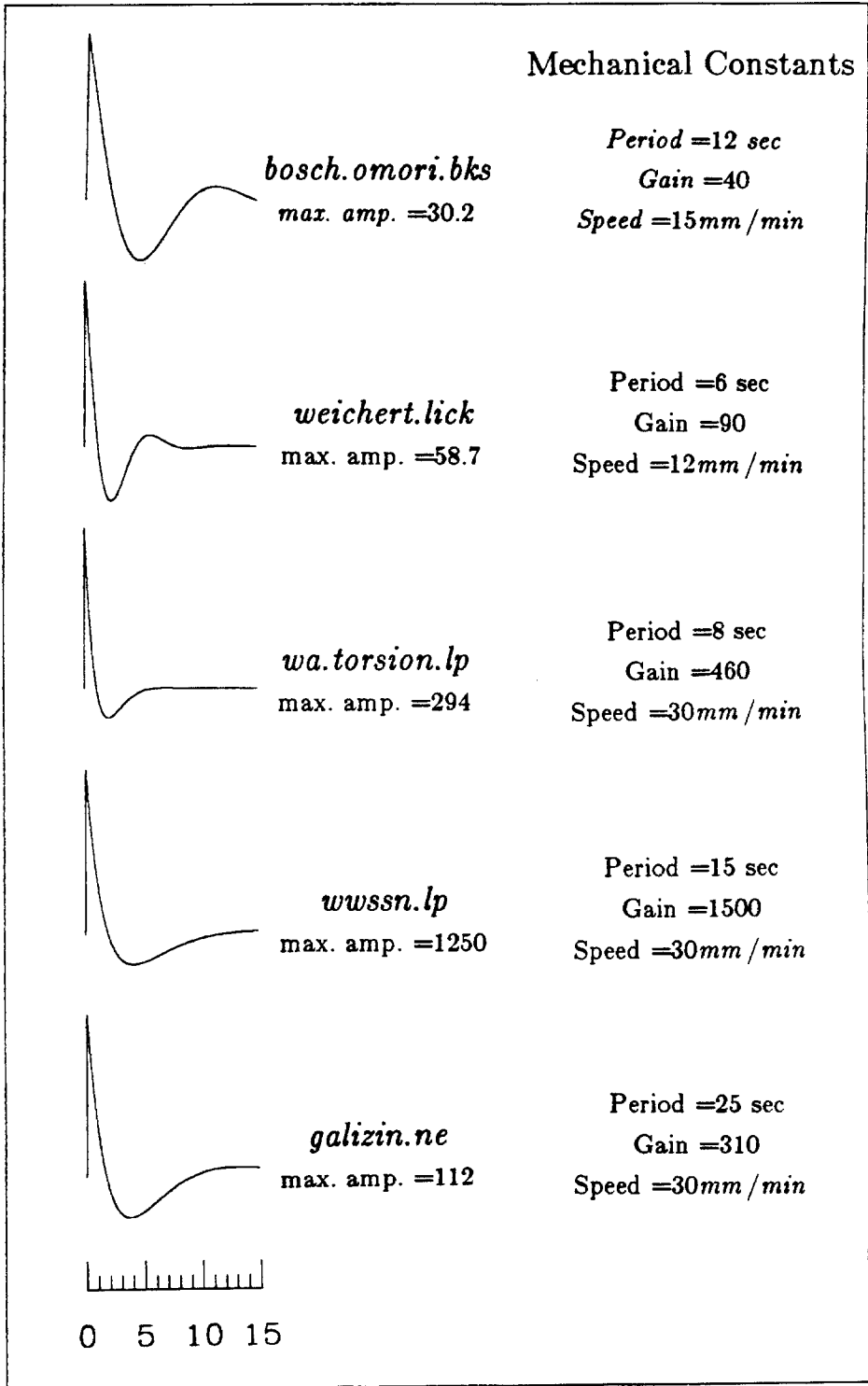


FIG. 3. Comparison of instrumental responses of historical seismographs with the standard worldwide long-period system. The Weichert response is underdamped. The drum speed and the instrument constants for these old seismographs are shown.

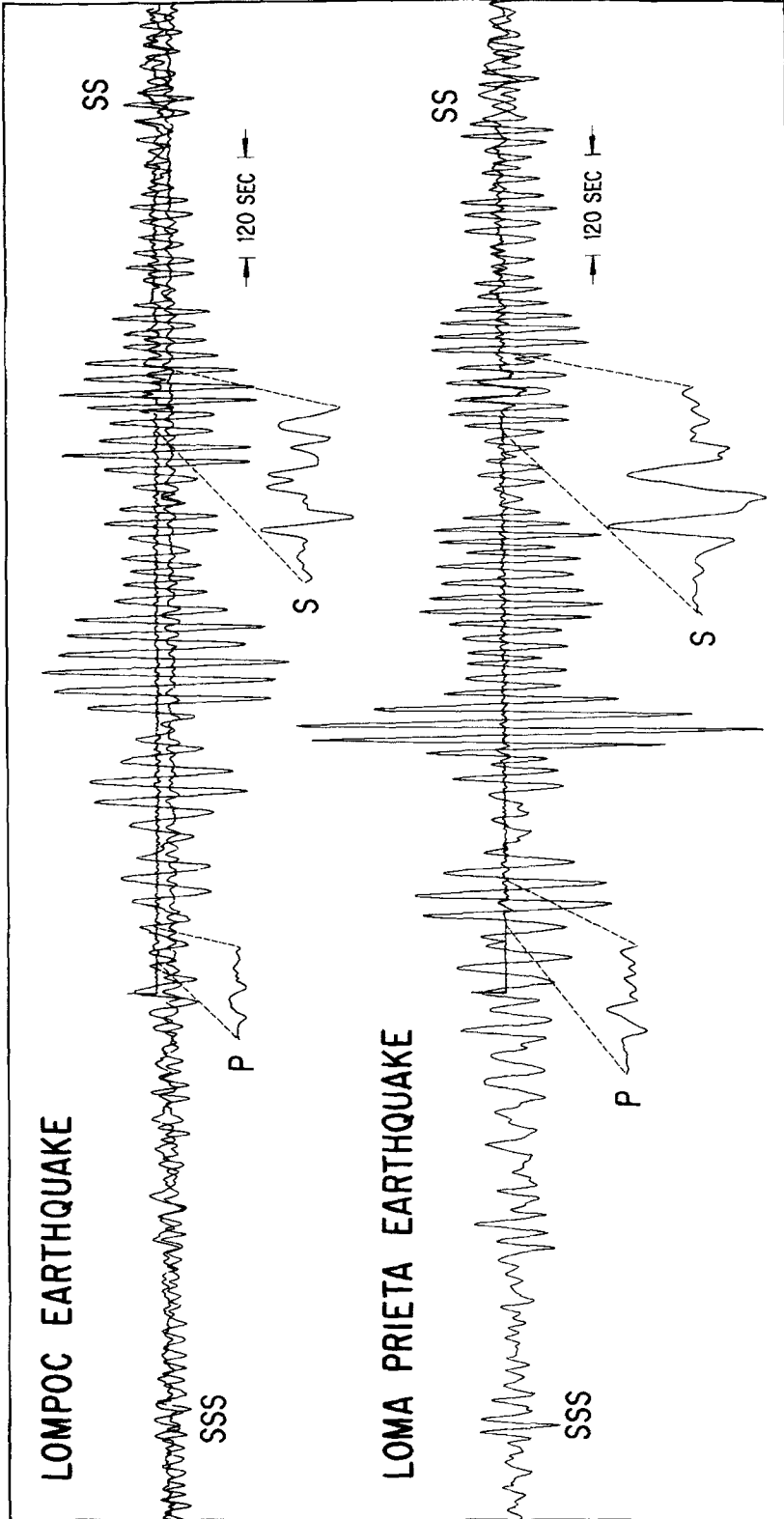


FIG. 4. Comparison of De Bilt EW component seismograms of the Lompoc and Loma Prieta events. The surface waves go slightly off-scale for the Loma Prieta event, which appears to be larger than the Lompoc event. *Insets* display enlarged phases ($\times 3$).

their original estimates of surface-wave magnitudes are equivalent to the 20-sec surface-wave magnitude M_s based on the WWSSN long-period instrument. These original estimates are to be found in the worksheets of Gutenberg and Richter, which have recently been archived by the Millikan Library at the California Institute of Technology and documented by Abe (1981). The worksheet for the Lompoc earthquake has 10 estimates of long-period body-wave magnitude obtained from five different stations, which give an average value of 7.3, and seven estimates of surface-wave magnitude, which give an average value of 7.0.

The surface-wave magnitude of the Lompoc earthquake relative to that of the Coalinga earthquake can be estimated by taking the ratio of peak surface-wave amplitudes averaged over the two horizontal components of the De Bilt seismograms. The ratio of approximately 4 yields an M_s difference of 0.6 units, giving an M_s estimate of 7.0 for the Lompoc earthquake based on the M_s of 6.4 for the Coalinga earthquake. This estimate is identical to the value measured by Gutenberg and Richter from seven teleseismic stations, as mentioned above.

The true ultra-long-period level of the type used in M_w (Kanamori, 1978) remains uncertain because of the inadequacy of the seismic stations in operation at that time. The best estimate of the long-period level is probably the value of 3×10^{26} dyne-cm ($M_w = 7.0$) obtained from tsunami data by Satake and Somerville (1992).

We will concentrate our efforts on defining the body-wave excitation and moment release associated with the shorter-period signals recorded by the older seismographs. In this study, we are primarily interested in locating the center of energy release rather than the hypocenter or the location of the initial rupture. Accordingly, we begin by modeling the seismograms to establish a criterion for best defining appropriate time picks to use in locating the centroid.

Synthetic seismogram methods have been widely used to analyze the source parameters of many recent Californian earthquakes using WWSSN and other global network stations. As a result of this experience, teleseismic travel paths between earthquakes in California and stations in Europe are quite well understood, allowing comparison of detailed features of earthquake sources. This allows us to make estimates of the source parameters of a sparsely recorded earthquake such as the 1927 Lompoc earthquake by comparing its seismograms with those of more recent earthquakes, such as the 1969 Santa Lucia Banks earthquakes, whose source parameters are well known.

Similarly, regional paths from known events to stations recording the Lompoc event, shown in Figure 2, can be modeled and used to fix parameters controlling path effects. Since this type of analysis is more difficult than teleseismic modeling, we give a brief review of this rapidly developing field.

REVIEW OF SOURCE PARAMETER ESTIMATION FROM REGIONAL BODY WAVES

Regional seismograms contain much more information about the source excitation than do teleseismic body waves because they sample much more of the focal sphere, but to retrieve this information requires separating out propagational complexities. Fortunately, by removing the shorter wavelengths, it becomes possible to explain the beginning portion of seismograms with relatively simple models. Figure 5 displays the comparison of synthetic seismograms with broadband seismograms of the 1988 Saguenay earthquake recorded by the Harvard Streckeisen instrument. The tangential component remains small for

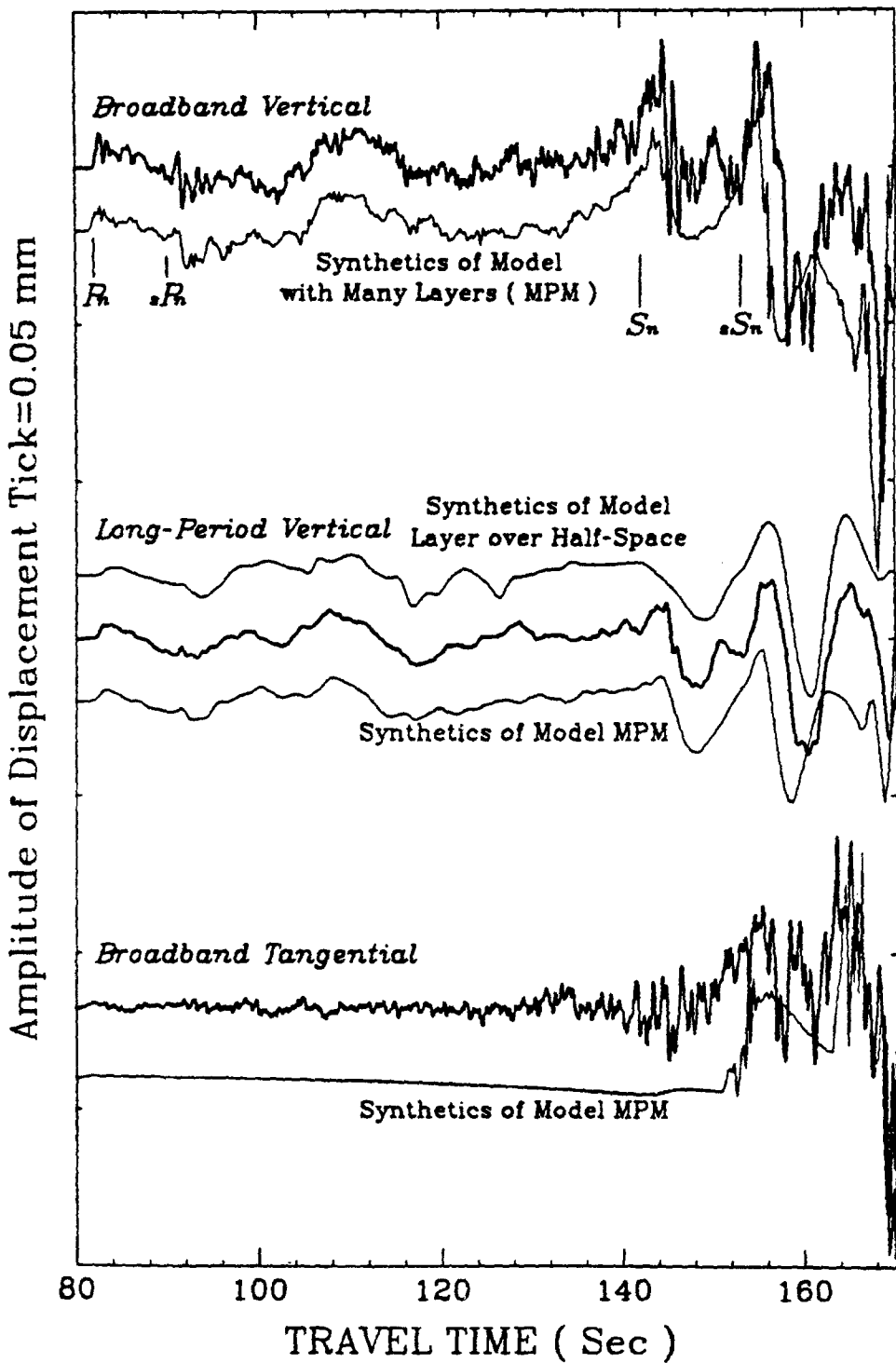


FIG. 5. Comparison of the broadband observations of the 25 November 1988, Saguenay, Quebec, earthquake as recorded at the Harvard station with synthetic seismograms. The *middle panel* displays the similarity between synthetic seismograms generated from a layer over a half-space with a multi-layered model (Table 1 and Zhao and Helmberger, 1991).

the first minute of the record while the vertical component displays the P wavetrain, consisting of Pn , pPn , sPn and PL . This early portion of the regional record has been labeled the Pnl wave for convenience (Helmberger and Engen, 1980), and shown to generally decompose into the (P - SV) and (SH) system of motions. The upper synthetic seismogram displays the results of a flat-layered modeling exercise with the five-layer crust (MPM) given in Table 1 of Zhao and Helmberger (1991). The middle two synthetic seismograms show the response after convolving with the long-period WWSSN response of Figure 3. This demonstrates that the synthetic seismograms for the simple one-layered crustal model fit quite well and are insensitive to crustal layering, as pointed out in several studies (Wallace and Helmberger, 1982; Liu and Helmberger, 1983; Bent and Helmberger, 1991).

The basic technique is developed in Helmberger and Engen (1980), who apply the point-shear dislocation approximation and assume that any earthquake can be constructed from a linear combination of three fundamental orientations displayed in Figure 6. Generally the dip-slip component shows the strongest sensitivity to depth, as shown in Figure 6. The short-period pulses correspond to crust-mantle reflections near critical angle, while the long-period pulses consist mostly of P headwave arrivals refracted along the top of the mantle. The robustness of the computational technique is due to insensitivity of the latter arrivals to variations in the crustal wave guide. The technique is most successful in tectonically stable regions and least successful along crustal margins, as shown in the mismatch in synthetics with data for paths from Santa Barbara to Corvallis, Oregon (COR) in Figure 7. Paths to Tucson, Arizona (TUC), from southern California seem to be well behaved, as found in other studies. Paths from southern California to Berkeley (BKS) are too short, causing the Pn and PL to be close together and nearly off-scale.

The same crustal model was assumed for all of these paths, giving rise to potentially significant travel-time residuals, as described by Helmberger and Engen (1980). However, the model can be perturbed to fit the Pnl waveforms and absolute travel times better if a calibration event is available. For instance, in Figure 8 we display the Loma Prieta broadband data and synthetic seismograms at Pasadena after calibrating the path against the previously studied neighboring Morgan Hill and Coyote Lake events (Liu and Helmberger, 1983). These synthetic and recorded seismograms are on the same time scale where we assume the origin times and locations reported by Dietz and Ellsworth (1990). The *upper half* of the figure displays the results for the 8 August 1989 preshock and the *lower half* the results for the mainshock. Included are comparisons of the broadband displacements and long-period torsion simulations (see Fig. 2), appropriate for the Tucson station. The agreement in timing between the recorded and synthetic seismograms demonstrates the effectiveness of the timing calibration derived from the Morgan Hill and Coyote Lake events. The gain of the instrument is included so that the height in cm is the expected height on a real seismogram. Thus the foreshock ($M = 5$) would be too small to be seen on a real (Wood-Anderson long-period torsion) instrument at Pasadena, while the main event ($M = 7$) would be off-scale. Nevertheless, these two events are quite similar in their long-period appearance except that they have different polarities at the start. The foreshock dips to the east while the main event dips to the west, which accounts for the Pn differences (Woods *et al.*, 1992). The entire Pnl waveform can only be nodal for pure strike-slip (Helmberger and

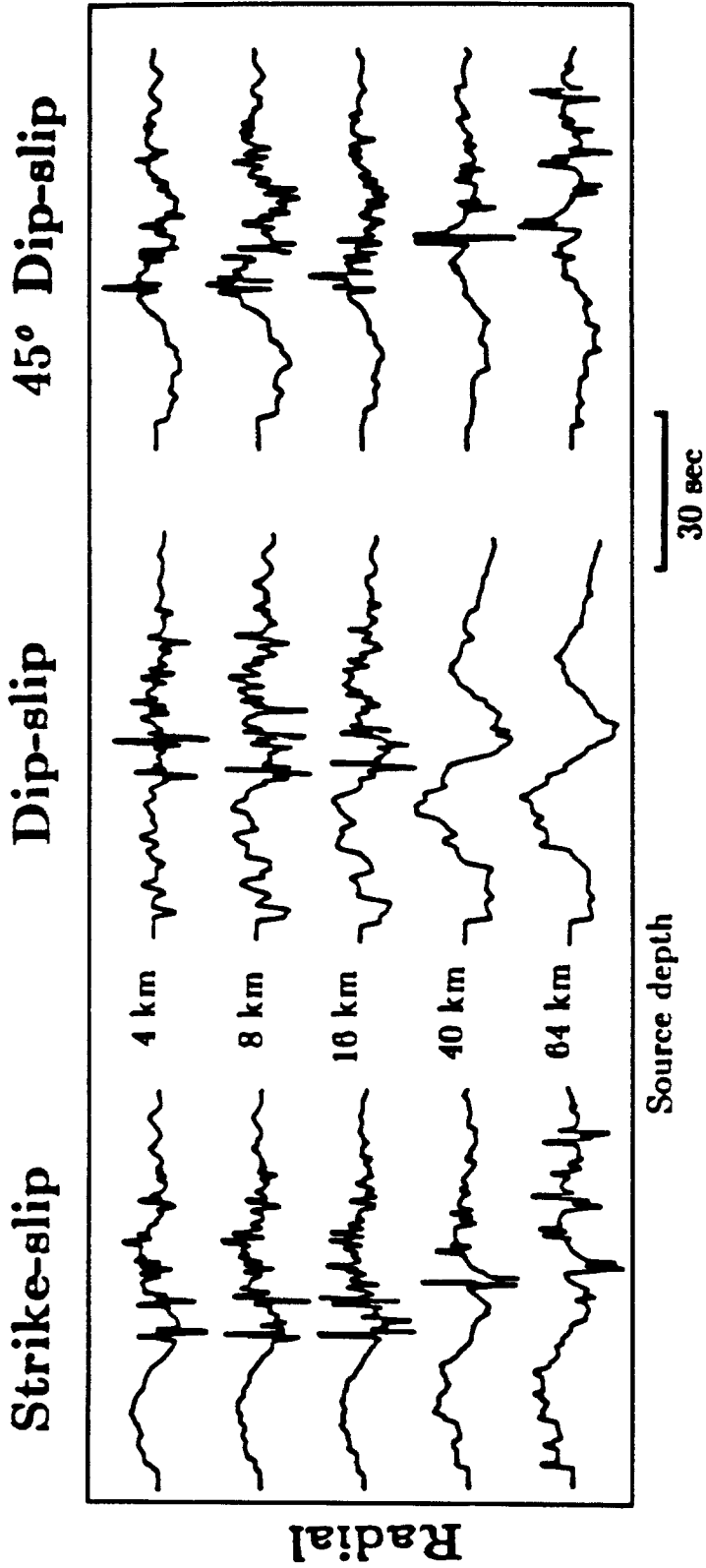


FIG. 6. Profiles of theoretical responses of a layer over a half-space as a function of source depth.

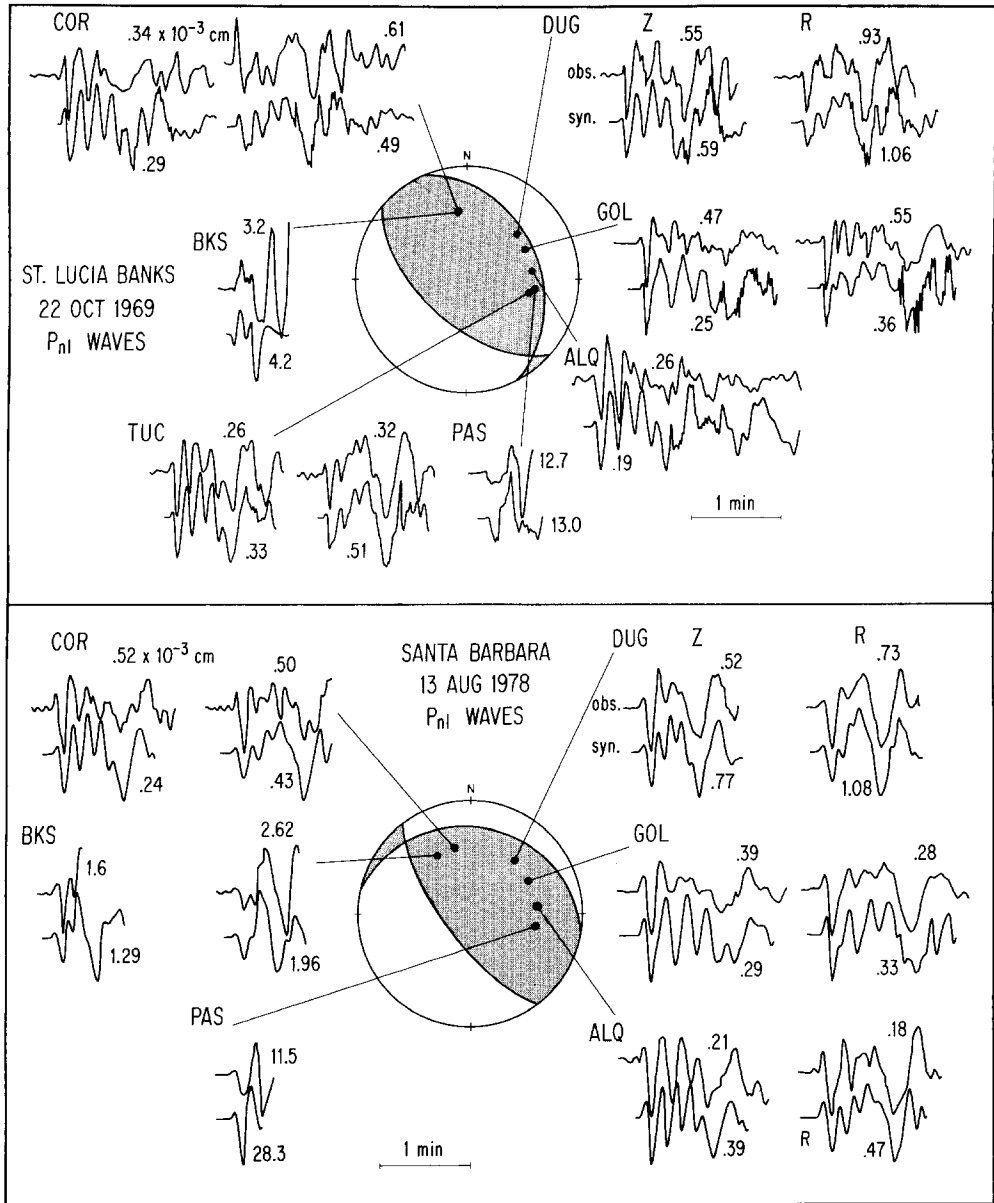


FIG. 7. Comparison of synthetic and observed seismograms of earthquakes along the oceanic-continent boundary (Bent and Helmberger, 1991). The amplitudes are indicated above each trace in cm (10^{-3}) where the instrumental gains have been removed.

Engen, 1980), which is why these regional seismograms are so useful in source mechanism determinations.

Although the contrast in data quality between Figures 2 and 8 is enormous, we can still use this modeling approach to help interpret the Lompoc data. First we note that the NS recording of the Lompoc main shock at BKS, which is essentially radial, has a strong *Pnl* waveform that looks like the BKS observation of the Santa Barbara event in Figure 7. The *Pnl* is compressional and the

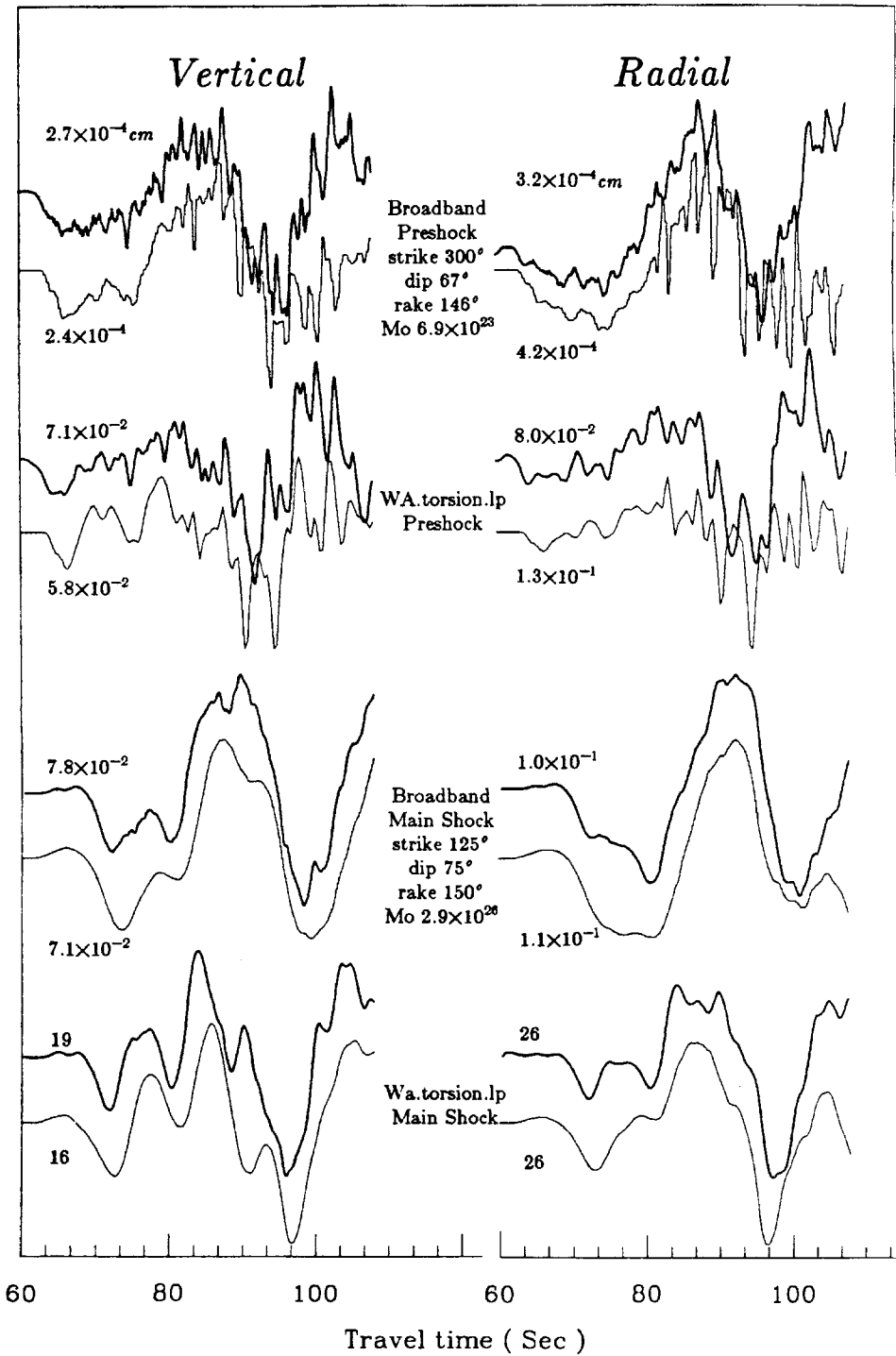


FIG. 8. Broadband Pn_l seismograms (*upper set*) and corresponding synthetic seismograms for a preshock (8/8/89 $M = 5$) and the Loma Prieta mainshock (10/18/89, $M = 7$). Pn is negative for the preshock and positive for the main event (Woods *et al.*, 1992). The *bottom* responses are appropriate for a long-period torsion instrument (TUC type in Fig. 3) where the peak amplitudes would be 0.13 cm for the preshock and 26 cm for the main event.

PL is strong. The *Pn* on the NS component at MHC looks negative or nodal. We conclude from this that *Pn* must be near a node along this azimuth. The radial *Pnl* portions of these records are displayed at the top of Figure 9, where we have included the MHC data, although we are giving it a low weight because of the uncertainty in its instrument response. By comparing the Lompoc and Santa Barbara events recorded at BKS, we can obtain an estimate of their relative source strengths. Note that the amplitude of the Santa Barbara event on the radial component is about 7.9 cm assuming the 1500 WWSSN gain (Fig. 7). Since the gain of the Bosch-Omori instrument is about 40 times smaller than the WWSSN system, we would estimate that the Lompoc event is roughly 30 to 40 times larger than the Santa Barbara event based on its *Pnl* at BKS. Similarly, the Loma Prieta event recorded at PAS produced 26 cm of amplitude on a Wood-Anderson long-period instrument, which would produce about 2 cm on a Bosch-Omori instrument. These comparisons suggest a moment from 1 to 2×10^{26} dyne-cm for the Lompoc earthquake, in agreement with the De Bilt comparisons with the Loma Prieta event shown earlier in Figure 4.

SEISMIC MOMENT AND FOCAL MECHANISM FROM BODY WAVES

In this section we compare the Lompoc records with those from neighboring events, using waveform modeling techniques as a guide in their interpretation.

Teleseismic Body Waves

The master events selected for comparison with the 1927 Lompoc earthquake are the 5 November 1969 magnitude M_s 6.0 Santa Lucia Bank earthquake and the 1983 magnitude M_s 6.4 Coalinga earthquake. The De Bilt seismograms for the 1927 Lompoc earthquake and these two more recent events are shown in Figure 10a. The similar *P*-to-*S* amplitude relationships of these seismograms suggest that the three events all have similar focal mechanisms. The large *P* amplitude relative to *S* is consistent with the reverse-slip mechanisms previously obtained for the 1969 and 1983 events.

Figure 10b shows the Lompoc and Coalinga *S*-wave recordings at De Bilt, with the horizontal components digitized and rotated to the radial and transverse components. The ratio of *SV* to *SH* has proven useful in determining focal mechanisms and was used by Choy (1985) in determining the focal mechanism of the Coalinga earthquake displayed in the upper panel of Figure 11. Since De Bilt is located near an *SH* node of the Coalinga event, we find a very small *S* arrival on the transverse component as predicted. The Lompoc seismogram shows a stronger *SH* arrival, and the lower panel of Figure 11 indicates the rotation in strike from 300° to 340° necessary to move the *SH* node away from De Bilt and match the recorded *SH* amplitude, as shown in Figure 12. If the mechanism of the Lompoc earthquake is purely dip slip, then the strike is constrained within 5° . Allowing some component of strike-slip would allow the strike to be more nearly north-south. This mechanism is compatible with nearly all of the polarity measurements (Stewart, 1979) available for the Lompoc earthquake, including the regional seismograms.

The match of the *SV* synthetic seismograms to the observed waveforms in Figure 12 is not particularly good, but this is not uncommon given *SV* receiver function complexities. Two types of distortions are common. The first is due to *SV*-to-*P* precursors introduced by the crust-mantle transition zone, which pro-

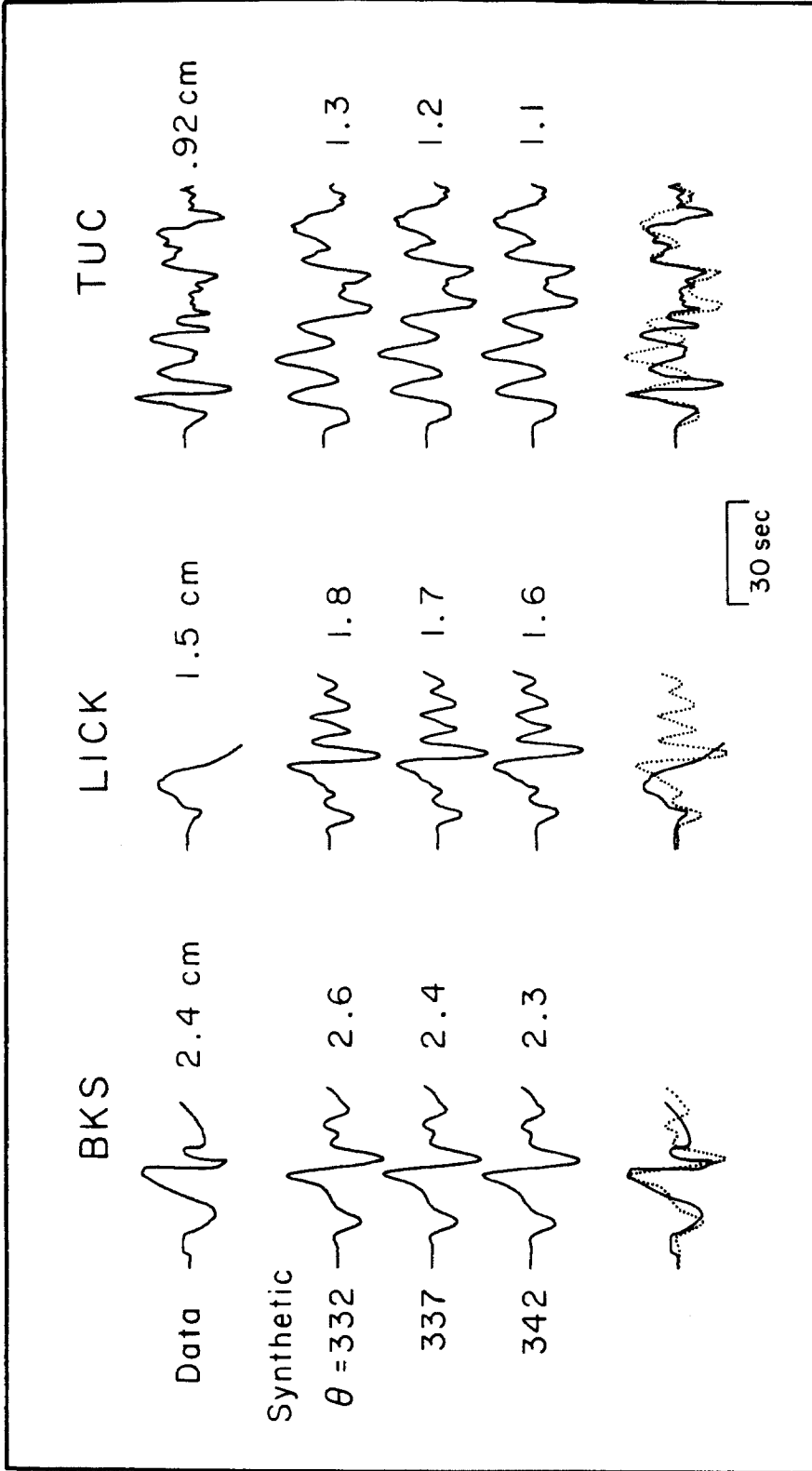


FIG. 9. Observed radial P_{nl} waves at the regional stations Berkeley, Lick Observatory, and Tucson compared with synthetic waveforms for three possible strike orientations, with fixed dip = 66° NE, and rake = 95° .

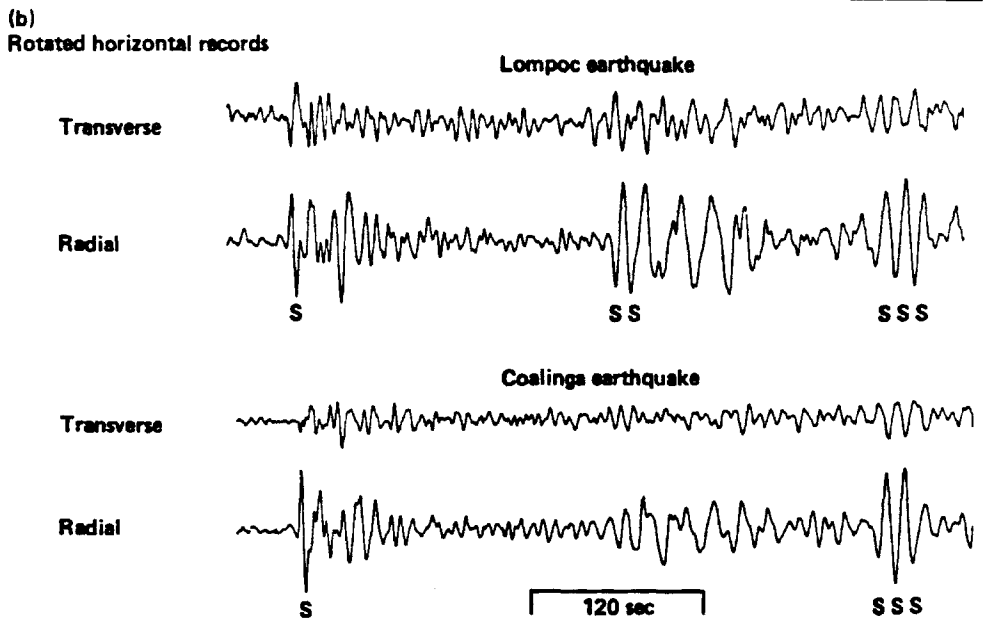
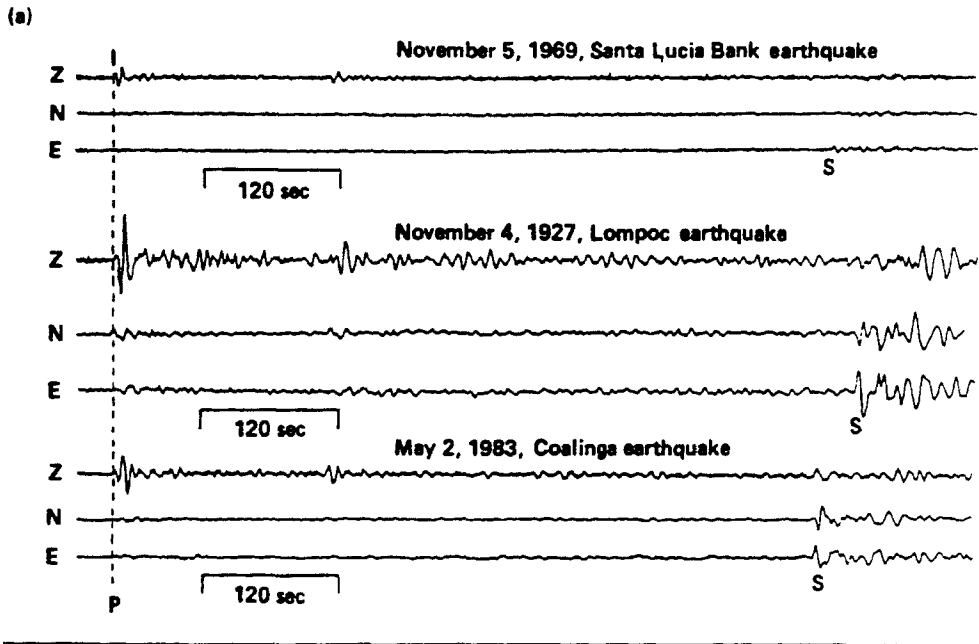


FIG. 10. (a) Comparison of seismograms observed at De Bilt, the Netherlands, for the 1927 Lompoc earthquake and two modern events. (b) Comparison of horizontal De Bilt seismograms of *S* waves rotated to transverse and radial components for the 1927 Lompoc and 1983 Coalinga earthquakes.

duces arrivals slightly ahead of the direct *SV* and opposite in polarity on the radial component (Burdick and Langston, 1977). The second complexity is produced by *PL*-coupled *SV* waves that arrive behind *S*, often off-azimuth. This feature is particularly common along oceanic-continental boundaries. The Coalinga synthetic seismograms are predictions from the source parameters

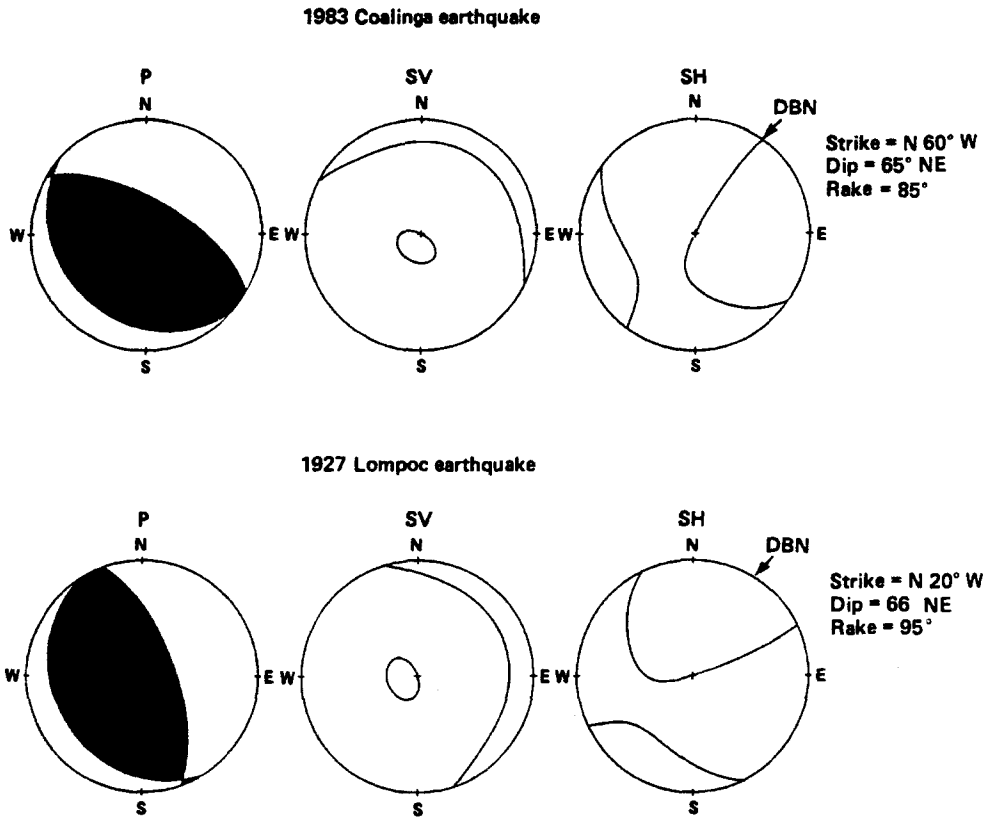
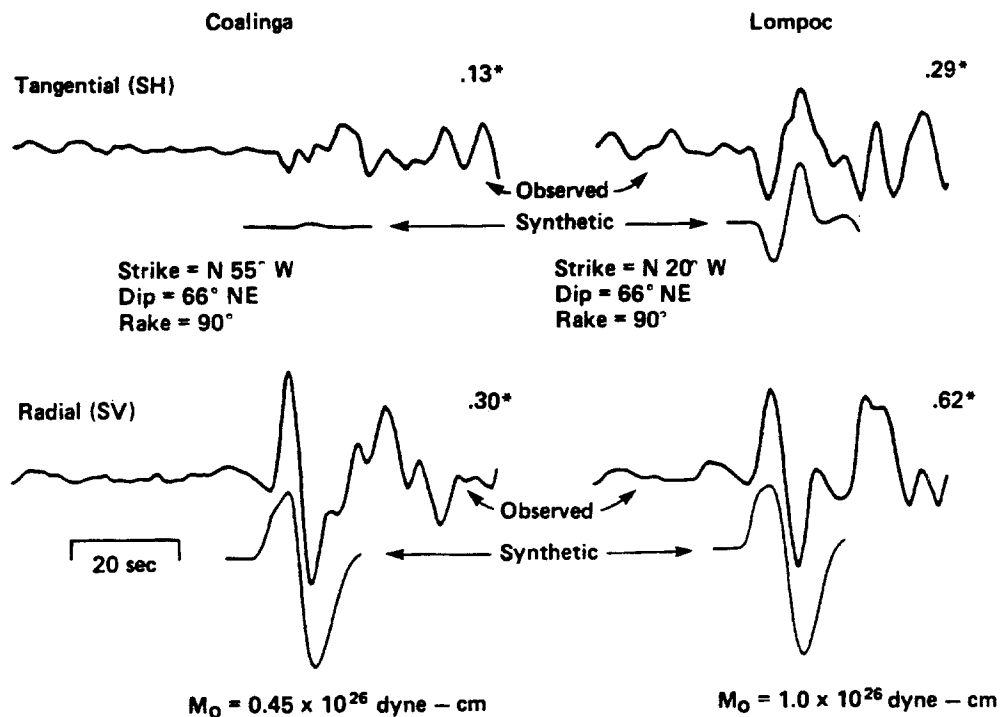


FIG. 11. Focal mechanism plots indicating nodal planes for P , SV , and SH for the 1927 Lompoc and 1983 Coalinga earthquakes. The azimuth to De Bilt (DBN) from the epicentral area is indicated for the SH plot.

given by Choy (1985) without attempting to model these receiver effects. The downward motion at the beginning of the observed SV waveform is probably this neglected P precursor. Thus, the predicted (S , pS , sS) synthetic interference is too broad, and we would expect, and in fact observe, a similar behavior for the Lompoc event. The difference in amplitude ratio of SH to SV between the two solutions displayed in Figure 12 is still meaningful in spite of these receiver complexities.

The source model of the Lompoc earthquake used in the S -wave synthetic seismograms of Figure 12 was derived from modeling the P waves shown in Figure 13, taking advantage of the detailed correspondence between the recorded seismograms of the Lompoc and Coalinga earthquakes. Forward computations were performed using this source model for the Coalinga event, the model of Bent and Helmberger (1991) for the Santa Lucia Banks event, and the model of Bent (1990) for a well-constrained Coalinga aftershock, to generate synthetic seismograms for comparison with the De Bilt recordings (Fig. 13). The relative timing of the P , pP , and sP phases strongly constrain the depth of the Lompoc earthquake to be very similar to that of the Coalinga earthquake, about 10 km. From the comparison of recorded and synthetic P waves of the two earthquakes, the Lompoc earthquake is estimated to have a seismic moment of 1.0×10^{26} dyne-cm, approximately twice that of the Coalinga mainshock. The



* Relative SH to SV Amplitudes

FIG. 12. Comparison of observed (rotated) *S* waves with synthetic waveforms for the 1927 Lompoc and the 1983 Coalinga earthquakes. The recorded peak amplitudes of the data are shown to the right of the traces. Both the data and synthetics for the Coalinga event have been scaled up by a factor of 2.2 to equalize the estimated seismic moments and facilitate comparison of the ratio of *SH* to *SV* motions for the two events.

duration of the Lompoc source is estimated to be 6 sec compared with the 5-sec duration of the Coalinga mainshock.

Regional Body Waves

Modeling regional seismograms is considerably more difficult than modeling teleseismic waveforms because of the complications of the crustal wave guide, as discussed earlier. However, by filtering out the higher frequencies, it becomes possible to explain the *Pnl* phase at the beginning of the seismograms. Normally, the moments obtained from regional records agree to within 25% of teleseismic estimates when the entire WWSSN array is operational (Wallace and HelMBERGER, 1982).

The true azimuth from the event to BKS is uncertain because of the location uncertainty and therefore the nodal position is equally uncertain. Synthetic seismograms covering a 10° range of azimuths are shown in Figure 9 using the focal mechanism at the bottom of Figure 11 and a seismic moment of 1.0×10^{26} dyne-cm. The sharpness of the nodal crossing in the synthetic seismograms is more subdued in the Berkeley and Lick seismograms than in the data. The close agreement between the recorded and synthetic seismograms for a strike direction of 340° , shown at the bottom of Figure 9, further confirms the nearly pure reverse mechanism of the 1927 Lompoc earthquake.

07/22/83

Coalinga aftershock



$M_0 = 0.5 \times 10^{25}$ dyne-cm
 $h = 8$ km
 $\delta t_s: 1, .5, 1$ sec

11/05/66

Santa Lucia Banks



$M_0 = 0.15 \times 10^{26}$ dyne-cm
 $h = 8$ km
 $\delta t_s: 1, 1, 1$ sec

05/02/83

Coalinga mainshock

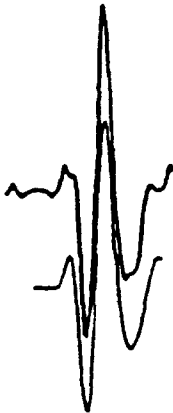


$M_0 = 0.45 \times 10^{26}$ dyne-cm
 $h = 10$ km
 $\delta t_s: 1, 3, 1$ sec

11/04/27

Lompoc

30 sec



$M_0 = 1.0 \times 10^{26}$ dyne-cm
 $h = 10$ km
 $\delta t_s: 2, 2, 2$ sec



EXPLANATION	
M_0	= Seismic moment
h	= Depth
δt_s	= Source time function
	= Observed
	= Synthetic

FIG. 13. Comparison of observed *P* waves with synthetic waveforms for the 1927 Lompoc November 1969 Santa Lucia Banks, and 1983 Coalinga earthquakes.

LOCATION FROM BODY WAVES

Gawthrop (1978a, b) used the reported travel times to locate the Lompoc event just off Point Sal at 34.9°N, 120.7°W (Fig. 1). To determine this location, he used station corrections that were estimated from a contoured station-residual map of the western United States. However, station travel-time residuals vary on a much finer scale than the contouring system employed by Gawthrop. This location technique is also subject to errors in clock times and variability in procedures used to pick arrival times and has been the subject of a considerable amount of controversy, as summarized by Hanks (1979).

To estimate the highly variable station residuals, we adopted a modified master-event technique. First we took recorded ISC arrival times for six NTS nuclear blasts for which the hypocentral parameters are independently known (HALFBEAK, GREELEY, BOXCAR, BENHAM, JORUM, and PIPKIN) and used these times to estimate teleseismic station residuals appropriate for an event originating in western North America. These initial station corrections were then used to determine an optimized relocation of the Santa Lucia Banks event of 5 November 1969. To minimize instability in the station residuals we used only teleseismic data. We relocated the Santa Lucia Banks event at 34.612°N, 121.358°W, approximately 7 km east of Gawthrop's (1978b) location of 34.63°N, 121.43°W. Because this is the nearest large, well-recorded event to the Lompoc event, it was judged to be the best master event available. Using this new location and the ISC arrival times for the Santa Lucia Banks event, we estimated station residuals appropriate for events in the Santa Lucia-Lompoc offshore areas. Only teleseismic ($\Delta > 30^\circ$) stations for which we had such station residuals were then employed in the final relocation of the Lompoc event. Using this set of station corrections, we found a location of 34.9°N, -120.9°W for the Lompoc event, shown as location TP (teleseismic *P* waves) in Figure 14. Unfortunately, the error ellipse remains too large (50 km) to be meaningful, a result similar to that suggested by Hanks (1979).

In an attempt to further constrain this solution, we adopted a hybrid tracking scheme also displayed in Figure 14. By fixing the origin time at a series of times, we reduce the number of variables and construct a locus of resulting epicenters. We then use the *Pnl* calibrated path to TUC as discussed above to further restrict the solution, which results in a location near that proposed by Hanks. Comparisons of recorded and synthetic waveforms at TUC that correspond to these locations and origin times are given on the right. The synthetics are delayed 4.0 sec relative to the model (Table 1) based on the use of the Santa Lucia Banks event as a timing calibration (Fig. 7). Since the European stations dominate the data set, we anticipated an accurate distance estimate to stations like De Bilt (DBN). Unfortunately, the error bars remain large because even by moving the epicenter around we cannot explain the large residuals at the European stations even for an epicenter yielding the smallest set of variances: COP (5.0 sec), DBN (2.5), EBR (5.2), HAM (-2.1), PUL (3.9), UPP (-4.4). The fact that 1 sec in travel time maps into a change in location of about 20 km illustrates the large uncertainty entailed in any approach that relies on absolute times. We therefore turn to differential times as suggested by Hanks (1979) as the best way to locate historical events.

Hanks (1979) used *S-P* times of aftershocks recorded at local stations in determining his location at 34.6°N, 120.9°W. This method assumes that the

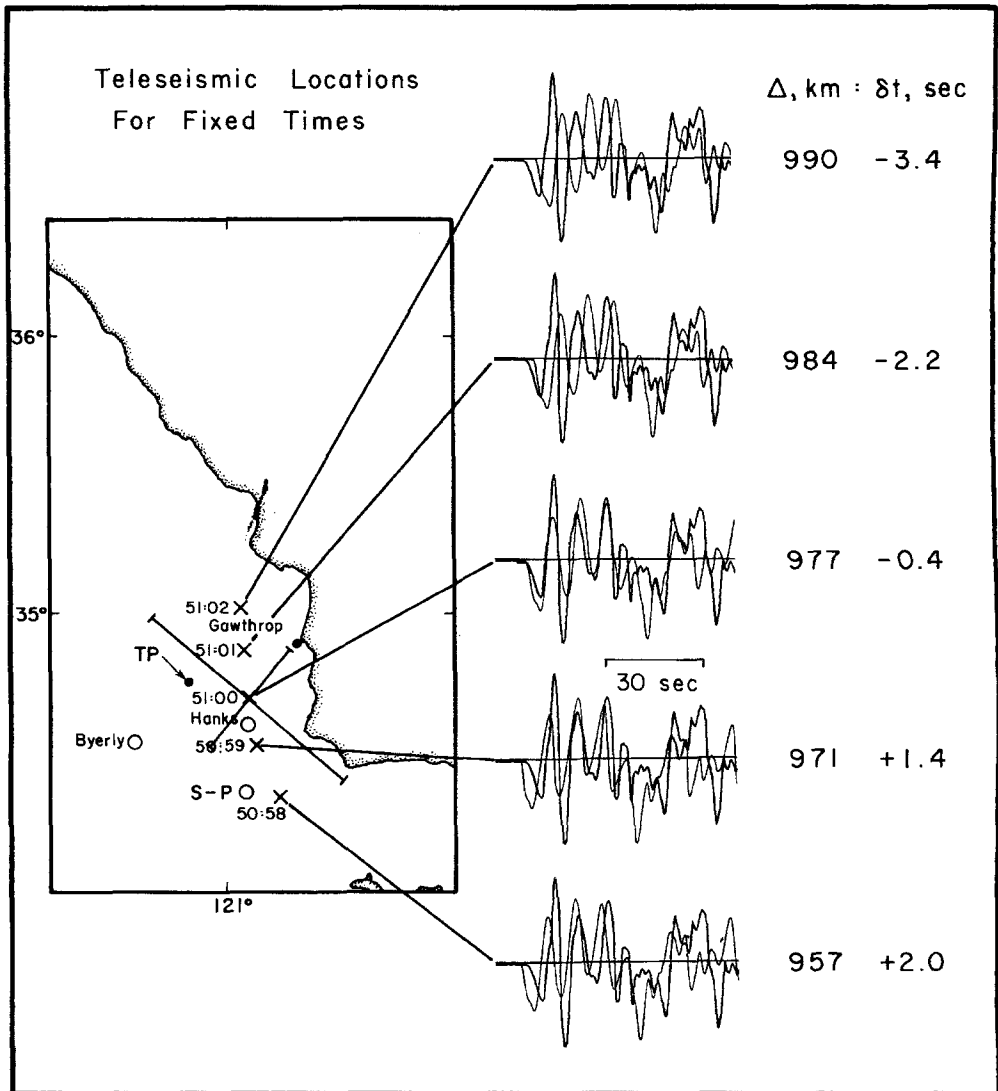


FIG. 14. Location TP is the best-fitting teleseismic location allowing the origin time to be a variable. The *left-hand plot* displays teleseismic locations as a function of assumed origin time. Comparisons of recorded and synthetic waveforms at TUC that correspond to these locations and origin times are given on the *right*.

aftershocks occurred in the same location as the mainshock. The *S-P* time arcs shown in Figure 1 (in the range of 12 to 14 sec) that he obtained from nearby SBC (Santa Barbara) were reread from the original records by us and seem unambiguous, providing a good constraint on the longitude of the location. An example is shown in Figure 15a. In this distance range (about 100 km), the first *P* and *S* arrivals are direct waves that propagate entirely within the crust (*P_g* and *S_g*). The *S-P* times were measured from both the NS and EW components for aftershocks with an impulsive *P* wave and a clearly visible *S*-wave onset. Of the approximately 390 aftershock *S-P* times cited in the unpublished California Institute of Technology (CIT) tables used by Hanks (1979), only 27 aftershocks met these criteria. However, the mean of our *S-P* times is 12.9 sec, which agrees

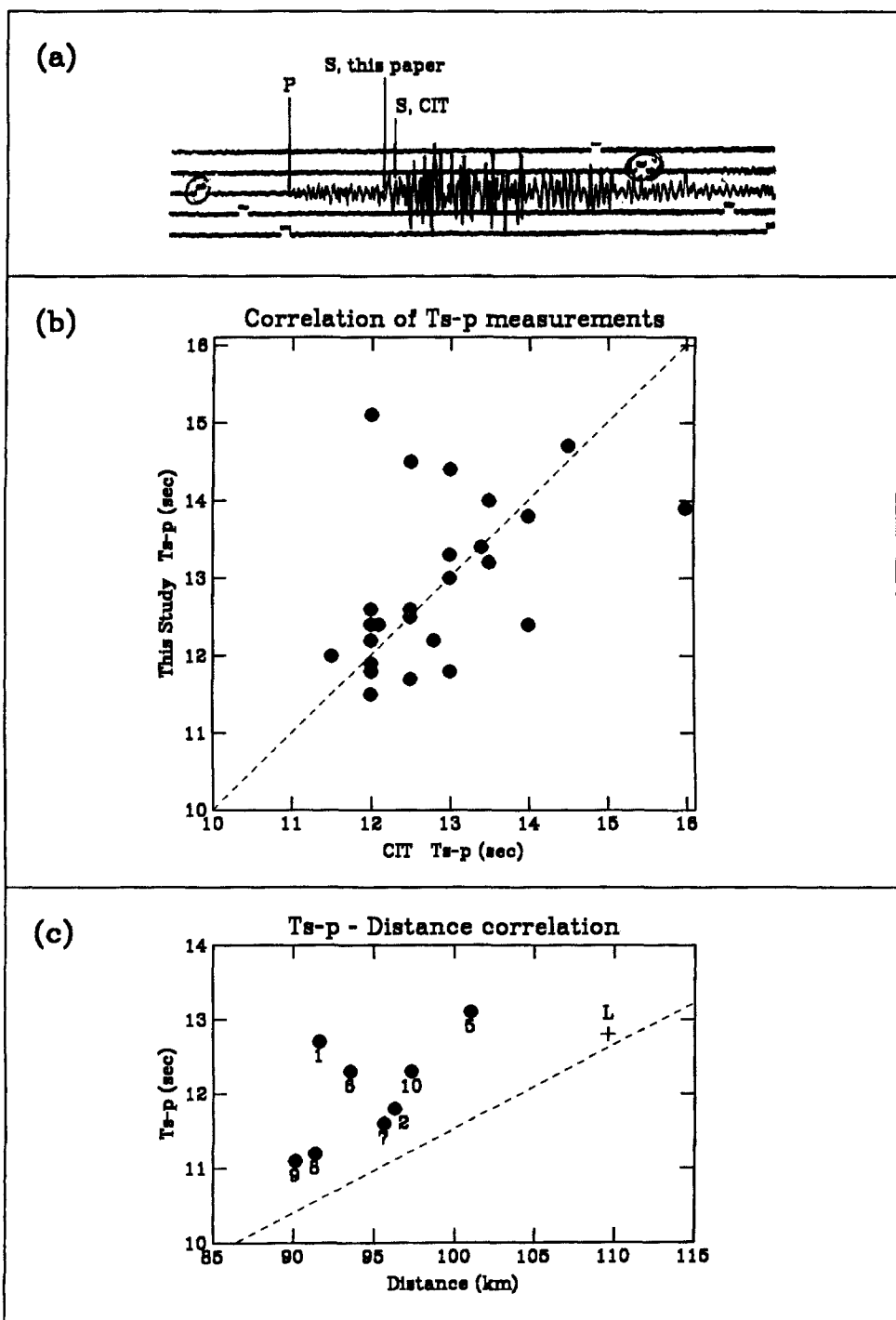


FIG. 15. (a) Example of a Santa Barbara recording of a Lompoc aftershock showing *S*-wave picks by CIT and by the authors. (b) Comparison of CIT and our *S*-*P* times at Santa Barbara for aftershocks of the 1927 Lompoc earthquake. (c) Comparison of *S*-*P* times at Santa Barbara for recent earthquakes off Point Conception with times predicted by the Richter (1958) curve. The 1927 Lompoc earthquake is indicated by an L.

TABLE 1
 T_{S-P} Times of November 1927 Lompoc Aftershocks
 Recorded at SBC

Date (m/d/y)	Time (Hr:Min)	T_{S-P} CIT (sec)	T_{S-P} (sec)
11/04/27	10:52	12	12.2
	16:17	16	13.9
	19:28	11.5 ±	12.0
	20:06	12.0	12.4
	20:43	12.0	12.6
	21:30	12.5	14.5
11/05/27	19:00	12.5	11.7
	20:26	12.8 ±	12.2
	20:51	13	11.8
	20:53	12.0 ±	12.4
	20:58	12	11.5
11/06/27	23:09	12.1	12.4
	01:05	13.4	13.4
	23:09	12.1	12.4
	02:40	13.5	14.0
	02:49	12.5	12.5
	04:49	14.5	14.7
	09:11	14	12.4
	09:39	12.0 ±	11.9
	12:02	12	11.8
	17:27	13	13.0
11/07/27	23:02	13	13.3
	01:30	12.5 ±	12.6
	03:43	13	14.4
	04:55	14	13.8
	06:20	13.5	13.2
	07:17	12	15.1

Time is approximate time of aftershock. CIT is the T_{S-P} time as it appears in the Caltech unpublished tables. The new estimate of T_{S-P} yields an average of 12.9 sec.

with the mean of the CIT times, 12.8 sec, cited by Hanks (1979). In Table 1, the times are listed together with the times originally read at CIT. The correlation between our times and the CIT times for the same events are shown in Fig. 15b. We do not see a systematic difference between the two sets of times.

Hanks (1979) used this $S-P$ time of 12.8 sec to draw an arc from Santa Barbara to locate the 1927 earthquake, using the travel-time curve of Richter (1958) for the southern California region. To evaluate this travel-time curve we read the $S-P$ times at Santa Barbara of more recent earthquakes that are located in the vicinity of the 1927 earthquake, specifically those larger than magnitude 3 occurring between latitude $34^{\circ}5'$ and $34^{\circ}35'$ and longitude $120^{\circ}35'$ and $121^{\circ}10'$ between 1980 and 1989, as listed in Table 2. The $S-P$ times are plotted against epicentral distance in Figure 15c, together with Richter's curve and the $S-P$ time of Hanks (1979). These results indicate that, west of Santa Barbara, the Richter curve overestimates the epicentral distance for a given $S-P$ time by less than 10 km on average, which is within the uncertainty of 10 km assigned to the 12.8 sec Santa Barbara arc as shown in Figure 1.

TABLE 2
S-P TIMES OF RECENT EARTHQUAKES OFF POINT CONCEPTION

Date (m/d/y)	Time (Hr:Min Sec)	Latitude	Longitude	Depth (km)	Magnitude	T_{s-p}
07/18/80	05:14 50.99	34N34.00	120W41.95	4.8	3.0	12.7
05/10/85	15:48 0.34	34N25.12	120W45.60	7.6	3.7	11.8
11/23/86	2:08 59.77	34N17.69	120W39.30	13.3	3.0	
02/27/87	22:43 19.32	34N31.00	120W46.51	0.0	3.6	
08/06/88	5:35 10.86	34N30.46	120W48.59	12.2	3.0	13.1
01/09/89	23:01 17.16	34N29.61	120W43.73	9.1	4.0	12.3
01/10/89	0:34 37.65	34N25.25	120W45.15	5.6	3.0	11.6
01/10/89	12:45 42.32	34N28.97	120W42.38	8.7	3.1	11.2
01/10/89	17:21 21.51	34N29.64	120W41.52	4.4	3.1	11.1
04/26/89	14:47 10.40	34N26.79	120W46.29	6.0	3.8	12.3

Byerly's S - P times for BKS are not so clear because of the difficulties in identifying regional phases such as P_n , S_n , \bar{P} , \bar{S} , etc., from larger events (Fig. 2). It is sometimes possible to identify certain phases on regional records such as these if one has a well-calibrated master event that is located by other means. This can be accomplished by comparative means or by numerical modeling of the type discussed earlier. Unfortunately, we were not able to establish a master event along this particular path. Second, the aftershocks recorded at BKS do not show a clear S arrival as is the case of the recording from the Santa Barbara event (Fig. 7). Another difficulty lies in the source complexity itself. It is common for events of this magnitude to begin with a small precursor, which is how we interpret the small first arrival on the BKS NS component and Z component. Byerly's origin time is 5 h/30 m/53 sec, which is 8 sec earlier than predicted by locations as far north as Gawthrop's. In short, the latitude constraint based on the BKS records is not very satisfactory, and we therefore return to a comparative study of the De Bilt records.

Teleseismic Body Waves

The similarity in waveforms between the Coalinga, Santa Lucia Banks, and Lompoc seismograms at De Bilt, which is due to their similarity in mechanism, depth, and seismic moment as discussed earlier, allows precise estimation of S - P and SSS - S times by overlaying and aligning the waveforms. We use these differential times to obtain a stronger constraint on the latitude of the location.

Location with respect to the Santa Lucia Banks Earthquake. The location of the 5 November 1969 Santa Lucia Banks event, as given by Gawthrop (1978a), is shown in Figure 1, and is estimated to have an uncertainty of less than 10 km based on our relocation as described above. The focal depth of the earthquake was estimated to be 8 km from depth phases; this depth is similar to the focal depth of 10 km estimated for the 1927 Lompoc and 1983 Coalinga earthquakes.

We have used SSS - S and S - P travel-time differences to estimate the location of the Lompoc earthquake with respect to the Santa Lucia Banks earthquake. The S - P interval that is used is measured from the onset time of P , which is clear for both events, to the first large peak of the S wave. We chose this peak rather than attempt to identify the S onset, because the S waves are dominated by SV and so their onsets are contaminated by P -to- S conversions as discussed

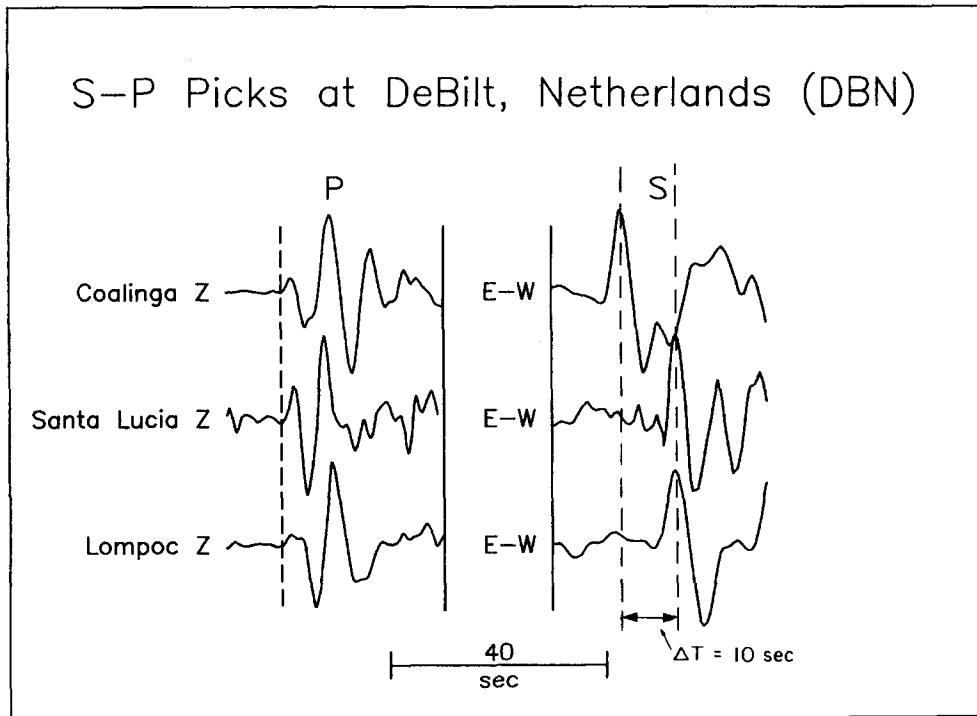


FIG. 16. Comparison of $S-P$ times of the 1927 Lompoc, November 1969 Santa Lucia Banks, and 1983 Coalinga earthquakes.

earlier. The $S-P$ times of the Lompoc and Santa Lucia Banks earthquakes are identical, as shown in Figure 16. The location of the Lompoc earthquake with respect to the Santa Lucia Banks earthquake according to this measurement lies on the small circle centered on De Bilt and drawn through the Santa Lucia Banks epicenter. The location of the Lompoc earthquake is established as the intersection of this arc with the Santa Barbara arc, shown in Figure 1.

The difference in $SSS-S$ interval between the Lompoc and Santa Lucia Banks earthquakes was measured by aligning the two S waves using cross-correlation, and then finding the time difference between the two SSS waves using cross-correlation, as shown in Figure 17. The $SSS-S$ time of Lompoc event is 0.5 sec greater than that of the Santa Lucia Banks event, placing the Lompoc earthquake about 12 km south of the location derived from $S-P$. The proximity of the Lompoc and Santa Lucia Banks earthquakes is reflected in the similarity of their waveforms; this is particularly evident when the Santa Lucia Banks record is lowpass filtered to provide a better comparison with the larger Lompoc earthquake.

Location with Respect to the Coalinga Earthquake. To check the location relative to the Santa Lucia Banks earthquake described above, we applied the same method to the Coalinga earthquake. We first used the known locations of the Coalinga and Santa Lucia Banks earthquakes (1.85° apart) and their measured $SSS-S$ time difference (9.3 sec) to estimate the relation between $SSS-S$ time difference and distance from Coalinga (5.0 sec per degree). Applying this to the $SSS-S$ time difference of 10.1 sec between the Coalinga and

SSS-S Picks at DeBilt, Netherlands (DBN)

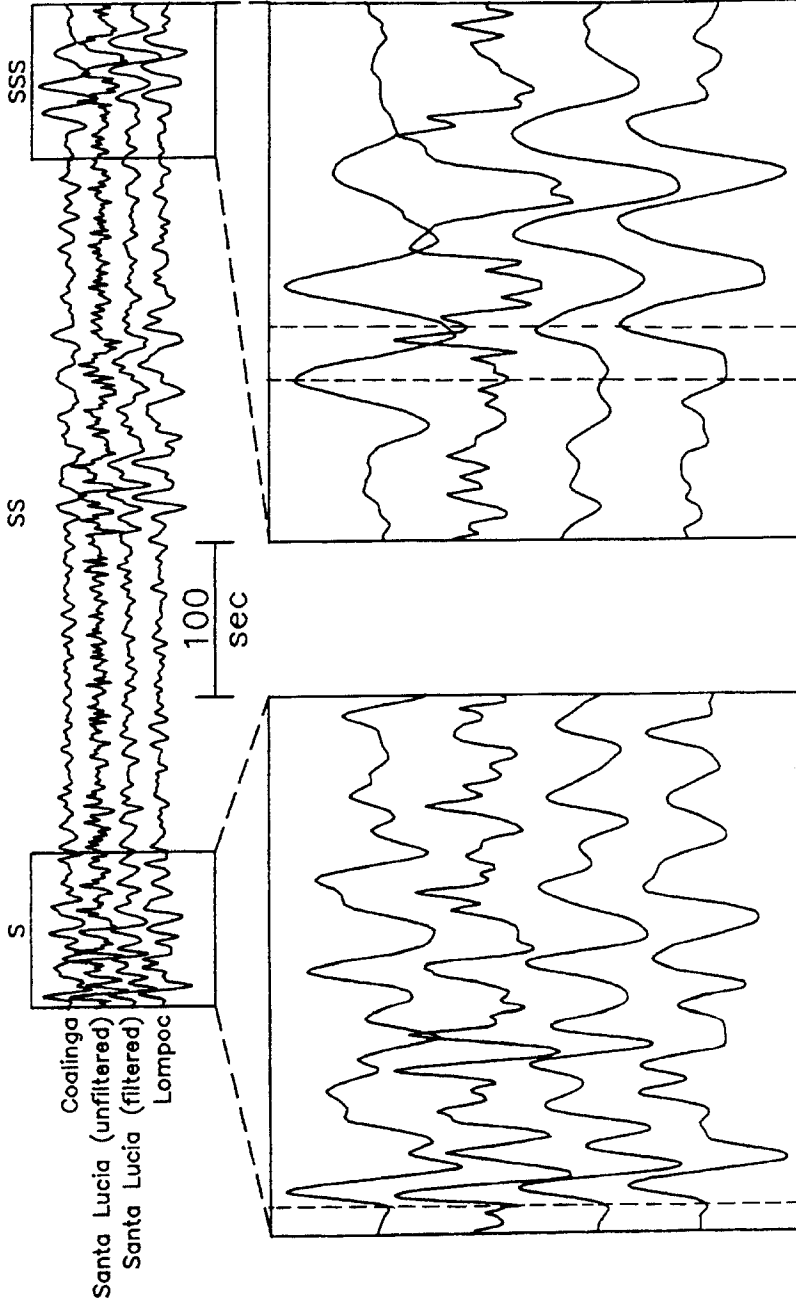


FIG. 17. (a) Comparison of shear-wave seismograms of the 1927 Lompoc, November 1969 Santa Lucia Banks, and 1983 Coalinga earthquakes, showing strong similarity in waveforms and timing of the Lompoc and Santa Lucia Banks events. (b) Comparison of SSS-S times of the three earthquakes. In the lower right box, the times of the first peak of the SSS wave for the Santa Lucia Banks and Lompoc events are seen to be similar, and approximately 10 sec later than that for the Coalinga event.

Lompoc earthquakes, as measured using the correlation method, places the Lompoc earthquake about 20 km south of the *S-P* location and about 10 km south of the *SSS-S* location with respect to the Santa Lucia Banks earthquake. The discrepancy of 10 km between the *SSS-S* locations of the Lompoc earthquake with respect to the Santa Lucia Banks and Coalinga earthquakes is a closure error and provides an indication of the level of uncertainty that is entailed in this measurement method.

The method of estimating *S-P* time uses simple time picks rather than cross-correlations and is thus not subject to closure error when the Coalinga earthquake is included in the analysis. The fact that the *S-P* times of the Lompoc and Santa Lucia Banks earthquakes are identical means that they both have the same difference in *S-P* time with respect to the Coalinga earthquake (10 sec) and their distances from Coalinga are thus identical. The *S-P* location of the Lompoc earthquake with respect to the Coalinga earthquake is thus identical to the *S-P* location of the Lompoc earthquake with respect to the Santa Lucia Banks earthquake.

Estimate of Location. Given the uncertainties discussed above, we conclude that the distance of the Lompoc earthquake from De Bilt is not significantly different from the distance of the Santa Lucia Banks earthquake from De Bilt. Together with the Santa Barbara arc, the De Bilt arc through the Santa Lucia Banks epicenter gives a location of 34.35°N, 120.9°W. This location lies about 25 km south of the Hanks (1979) location, but within the uncertainty of that location.

Regional Body Waves

Some additional constraints on location can be obtained from regional analyses. The largest uncertainty in the location is in its latitude, but we have seen that station BKS to the north does not provide satisfactory constraint on the latitude. Accordingly, we have used stations to the east of the epicentral regions to constrain the azimuth to the event. Although recordings from the short-period Wood-Anderson station at Santa Barbara are available, the mainshock recording is not. However, mainshock recordings on the short-period Wood-Anderson are available at Pasadena (PAS), and this station has the added advantage of also having long-period Wood-Anderson and Benioff (1-90) recordings of modern events. Accordingly, we have used PAS in our analyses of azimuth to the 1927 Lompoc earthquake.

Several events in and near the Lompoc area, including the Lompoc mainshock and one large aftershock, were analyzed. All available north-south (NS) and east-west (EW) ground motion recordings at PAS were digitized and analyzed for the following earthquakes: Lompoc mainshock and a large aftershock occurring on 5 November 1927; Point Conception (27 August 1949 at 34.5°N, 120.5°W, from Hileman *et al.*, 1973); two Santa Lucia Banks earthquakes (22 October 1969 at 34.77°N, 121.35°W, and 5 November 1969 at 34.72°N, 121.28°W, from ISC); and Point Sal (29 May 1980 at 34.98°N, 120.71°W, from Eaton, 1984). All available horizontal recordings from the long-period Benioff 1-90, long-period Wood-Anderson (W-A) 6-sec torsion, and short-period W-A 0.8-sec torsion were used. Four sets of records are displayed in Figure 18a. All four of the events shown have a very similar azimuth to PAS (between 279° and 283°), thus yielding similar waveforms, especially at long periods. The epicentral distances range from about 220 km (Pt. Conception) to about 290 km (Santa Lucia

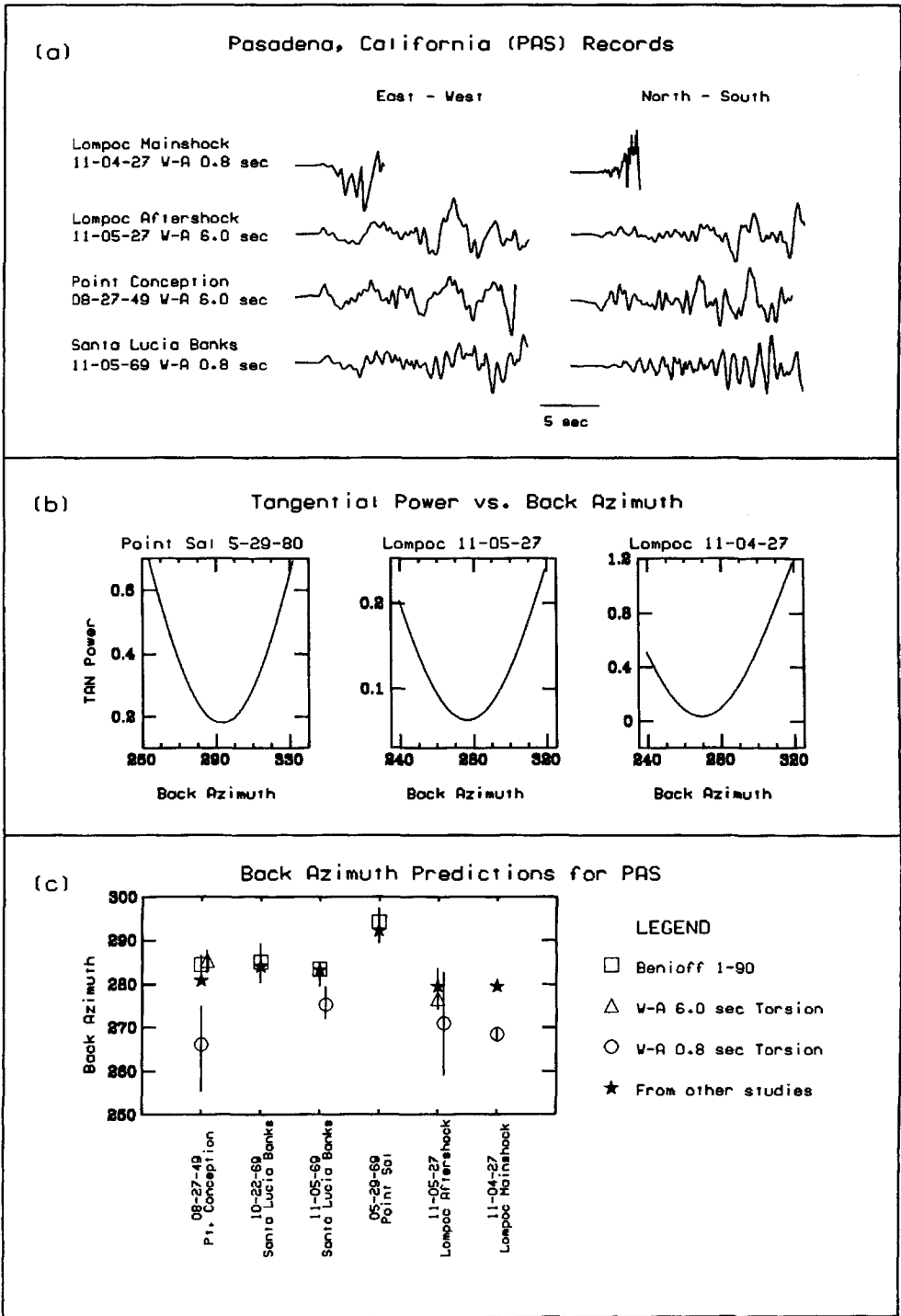


FIG. 18. Panel (a) displays the EW-NS components of the Lompoc mainshock and aftershock, the Point Conception 1949 event (from Hanks, 1979) and the Santa Lucia Banks (11/05/69) event. Panel (b) shows the method of backazimuth estimation. Panel (c) shows the comparison of estimated backazimuths with those of independently determined locations.

Banks). The first arrival is a Pn wave, which in all cases is clearly above the noise level.

The Pn wave was analyzed to obtain an estimate of a backazimuth vector from PAS to each event listed above. This was done by rotating a digitized pair of horizontal records to obtain the tangential (TAN) and radial components, then summing the squares of the TAN component over a certain time window (T) starting from the beginning of Pn , then dividing by T to obtain an estimate of power on the TAN component, that is,

$$\frac{1}{T} \sum_{n=1}^N (\text{TAN}_i)^2.$$

An algorithm was constructed to minimize this power by varying the backazimuth (BAZ) by plus or minus 40° from the BAZ of an assumed location for the given event. This was done as follows: for each BAZ, (1) rotate the records to obtain the TAN component, (2) compute the unit power, then (3) save the BAZ associated with the minimum TAN power. The assumed location for this algorithm merely sets the bounds of BAZ (plus or minus 40° to the assumed location) used in this calculation and is not related to the resulting BAZ associated with the minimum TAN power. This calculation is then carried out for different shifts in the NS record (-0.2 to $+0.2$ sec) prior to rotation in order to accommodate possible error in the time origin of the record from the digitizing process. This time shift prior to rotation also accommodates a time shift error between the original horizontal components, although the instruments at PAS were well calibrated in 1927, so this is not expected to be relevant. Many different lengths of the time window T were tried with this method. It was found that $T = 2$ sec gives the most accurate estimates of BAZ for events where the locations are well known (i.e., Pt. Sal and both Santa Lucia Banks events). This result is not surprising since the first half cycle of the Pn wave for this data set is about 2-sec long.

The minimum in the computed TAN power versus BAZ curve is robust, as illustrated in Figure 18b. Curves are shown for three events, each recorded on a different instrument: Pt. Sal (Benioff 1-90), the large 1927 aftershock (Wood-Anderson 6-sec torsion), and the 1927 mainshock (Wood-Anderson 0.8-sec torsion). The assumed locations were 34.98°N , 120.71°W for Pt. Sal, and $(34.50^\circ\text{N}$, $120.90^\circ\text{W})$ for both 1927 Lompoc events. The minima in these three curves represent the BAZ solution for this method.

The backazimuth vector results are summarized in Figure 18c. The solid stars are from the locations cited above, and the open symbols are BAZ estimates from this study. The results from the different instruments are shown as different open symbols, with the error bars signifying the uncertainty due to digitizer error in time origin placement on the record by the ± 0.2 sec NS record shift before rotation. The estimates from the long-period data (Benioff 1-90) and W-A 6-sec torsion) agree quite well with those from the assumed locations. The Pt. Conception BAZ estimates from long-period recordings are almost 5° larger than our assumed location BAZ, but this event occurred in 1949 and its location (34.5°N , 120.5°W) is less precise. However, both Santa Lucia Banks events (34.77°N , 121.35°W for the mainshock; 34.72°N , 121.28°W for the aftershock) and the Pt. Sal event have BAZ estimates from long periods that are very close to those of the assumed locations. For the Lompoc aftershock, the long-period

BAZ calculation is very close to our mainshock location BAZ, with the uncertainty bar encompassing this location. A significant finding here is that the aftershock BAZ calculation is much different from that of the Pt. Sal event; the latter is close to Gawthrop's (1978) location for the Lompoc mainshock.

The short-period BAZ estimates are consistently smaller than those from the long-period estimates and from assumed locations. This is probably due to receiver effects at PAS. Unfortunately, the only existing PAS records for the Lompoc mainshock are the short-period Wood-Anderson recordings. The BAZ estimate for the mainshock of 269° is about 11° smaller than that for our location, consistent with the difference in BAZ estimates from assumed locations using short-periods of the other events (Fig. 18c). If we increase the BAZ estimate for the Lompoc mainshock by 11° , which is the average difference between assumed values and those estimated from short-period Wood-Anderson seismograms for the Pt. Conception and Santa Lucia Banks (5 November 1969) events, we obtain an azimuth of 280° . This azimuth intersects the Santa Barbara *S-P* arc of Hanks (1978) at a latitude of 34.35°N at a point that is near to the location of the Lompoc mainshock derived from *S-P* times at De Bilt, as shown in Figure 1.

We conclude that the particle motions of *Pn* waves recorded at Pasadena are consistent with the latitude of our location of the Lompoc mainshock and inconsistent with the latitude of Gawthrop's (1978b) location near Pt. Sal.

Estimate of Uncertainty in Location. The uncertainty in location of the Lompoc earthquake cannot be less than that of the master events used in its location. For the Santa Lucia Banks earthquake, this uncertainty is estimated to be less than 10 km, while for the Coalinga earthquake it is a few km. In addition to this uncertainty is the variability in location obtained using different master events and different phase pairs, which is 10 km about the average location. Differences in such parameters as focal depth, earth structure, and source functions of the earthquakes are expected to give rise to additional uncertainty. We estimate the combined uncertainty of the location to be 25 km.

DISCUSSION

The location, focal depth, focal mechanism, and source strength of the 1927 Lompoc earthquake have been estimated using regional and teleseismic body-wave recordings. The location constraints were provided largely by differential travel times at two stations (De Bilt and Santa Barbara) using master event techniques. Our results indicate that the 1927 Lompoc earthquake sequence occurred on a north-northwesterly striking fault located about 40 km west of Point Conception, 34.35°N and 120.9°W . This location agrees with the recent tsunami modeling of Satake and Somerville (1992), who determined that this event occurred beneath at least 200 m of water near the same coordinates.

Because of the large epicentral uncertainty and the distance offshore, it is difficult to conclusively associate this earthquake with a specific geological structure. While it is possible that the earthquake occurred within the southern Santa Lucia Bank high, or in the offshore southern Santa Maria Basin, it appears most likely that the earthquake occurred along the southern Santa Lucia Bank fault zone that separates these two terranes. The epicenter is within the zone of surface faults identified by McCulloch (1987) as the southern extension of the Santa Lucia Bank fault zone. Although they were located in the

area of the western Santa Lucia Bank high, the two 1969 earthquakes also had compressional focal mechanisms, similar to the 1927 Lompoc earthquake.

The focal mechanism of the Lompoc earthquake was determined by comparing the body waveforms at De Bilt and regional records against similar records from modern events. The ratio of SV to SH at De Bilt and the relatively nodal Pn at BKS provided the major constraints, allowing a nearly pure dip-slip solution (rake = 95°) on a plane striking $N20^\circ W$ and dipping 66° NE. The seismic moment estimate derived from the body waves at De Bilt and the Pnl waves at BKS and TUC is $M_0 = 1. \times 10^{26}$ dyne-cm. Yeh (1975) obtained a value of 4.5×10^{26} for our orientation based on short-period Rayleigh wave spectra at De Bilt. However, since this value is larger than that for Loma Prieta ($M_s = 3 \times 10^{26}$ dyne-cm), we suspect that her estimate using 15-sec surface waves is biased high given the comparison of seismograms in Figure 4. Hanks *et al.* (1975) obtained a moment of 1×10^{27} dyne-cm by comparing the on-scale portion of the BKS records (Fig. 2) with the 1925 Santa Barbara records using the AR method, and using the areas of intensity VI. Based on recent strong-motion studies (Hanks and Johnston, 1992; Wald *et al.*, 1990), we would expect intensity patterns to be more related to stress drop and asperity distributions than to moment. Nevertheless, comparative studies of historical records at BKS and elsewhere are very important and will become increasingly so with the advent of the new Streckeisen seismographs. Unfortunately, many of the valuable historical records are no longer available.

CONCLUSIONS

This study reviewed the various recorded seismic data available from the 1927 Lompoc earthquake sequence including both regional and teleseismic seismograms. By analyzing the data together using waveform characteristics and travel-time differentials, we were able to develop a consistent picture of both the location and mechanism.

For the location, $S-P$ times from a large number of the 1927 aftershocks recorded at Santa Barbara compared with recent well-located events in the vicinity provided the longitudinal control. The latitudinal control comes from the differential travel times ($S-P$ and $SSS-S$ phases) of the main event recorded at De Bilt relative to the November 1969 Santa Lucia Banks event, which appears to be almost identical. These two arcs locate the event at $34.35^\circ N$ and $120.9^\circ W$ with an uncertainty of 25 km. A detailed analysis of the backazimuth estimates of horizontal motions recorded at Pasadena for both the main event and aftershocks supports this location, indicating that the main event did occur near its aftershocks.

The magnitude and fault orientation determination also involved a multiple approach, using direct comparisons of the 1927 waveform data with those from master events, and theoretical modeling analyses of the regional and teleseismic data. A consistent mechanism having nearly pure reverse faulting (strike = $N20^\circ W$, rake = 95° , and dip = $66^\circ NE$) was obtained. It is difficult to make a formal error analysis, but we estimate the uncertainty in these angles to be within $\pm 10^\circ$ by trial-and-error sensitivity tests. Synthetic fits to the teleseismic P -waveform data suggest a depth of 10 km. The regional and teleseismic results both indicate a moment of 1×10^{26} dyne-cm with a relatively short time history, about 6 sec, suggesting a source dimension of about 30 km. The surface-wave magnitude from the Gutenberg and Richter work sheets is 7.0.

ACKNOWLEDGMENTS

We would like to thank Allison Bent, Larry Burdick, Gladys Engen, Jim McLaren, and Lianshe Zhao for assistance and for reviewing this manuscript. Support for this study was provided in part by Pacific Gas and Electric Company and by USGS contract number 14-08-0001-G1872 at the California Institute of Technology, Division of Geological and Planetary Science contribution no. 4992.

REFERENCES

- Abe, K. (1981). Magnitudes of large shallow earthquakes from 1904–1980. *Phys. Earth Planet. Interiors* **27**, 72–92.
- Bakun, W. H. and T. V. McEvilly (1984). Recurrence models and Parkfield, California, earthquakes. *J. Geophys.* **89**, 3051–3058.
- Bent, A. L. (1990). Source characteristics of recent and historic earthquakes in central and southern California: results from forward modeling. *Ph.D. Thesis*, California Institute of Technology, Pasadena.
- Bent, A. L. and D. V. Helmberger (1991). Seismic characteristics of earthquakes along the offshore extension of the western transverse ranges, California. *Bull. Seism. Soc. Am.* **81**, 399–422.
- Burdick, L. J. and C. A. Langston (1977). Modeling crustal structure through the use of converted phases in teleseismic body-waveforms. *Bull. Seism. Soc. Am.* **67**, 677–691.
- Byerly, P. (1930). The California earthquake of November 4, 1927. *Bull. Seism. Soc. Am.* **68**, 53–66.
- Choy, G. (1985). Source parameters of the Coalinga California earthquake of May 2, 1983 inferred from broad-band waves. *U.S. Geol. Surv. Open-File Rep. 85-44*, 83–105.
- Dietz, L. D. and W. L. Ellsworth (1990). The October 17, 1989, Loma Prieta, California earthquake and its aftershocks: geometry of the sequence from high-resolution locations. *Geophys. Res. Lett.* **17**, 1417–1420.
- Eaton, J. P. (1984). Focal mechanisms of near-shore earthquakes between Santa Barbara and Monterey, California. *U.S. Geol. Surv. Open-File Rep. 84-477*.
- Feigl, K. L., R. W. King, and T. H. Jordan (1990). Geodetic measurement of tectonic deformation in the Santa Maria fold and thrust belt, California. *J. Geophys. Res.* **95**, 2679–2699.
- Gawthrop, W. H. (1978a). Seismicity and tectonics of the central California coastal region, in *San Gregorio-Hosgri fault zone, California*, E. A. Silver and W. R. Normack (Editors), *Calif. Div. Mines Geol. Spec. Rep.* **137**, 45–56.
- Gawthrop, W. (1978b). The 1927 Lompoc, California earthquake. *Bull. Seism. Soc. Am.* **68**, 1705–1716.
- Gawthrop, W. H. (1981). Comments on “The Lompoc, California, earthquake (November 4, 1927; $M = 7.3$) and its aftershocks” by Thomas C. Hanks. *Bull. Seism. Soc. Am.* **71**, 557–560.
- Geller, R. J. and H. Kanamori (1977). Magnitudes of great shallow earthquakes from 1904 to 1952. *Bull. Seism. Soc. Am.* **67**, 587–598.
- Gutenberg, B. and C. F. Richter (1956). Magnitude and energy of earthquakes. *Ann. Geophys. (Rome)* **9**, 1–15.
- Hanks, T. (1979). The 1927 Lompoc, California earthquake (November 4, 1927; $M = 7.3$) and its aftershocks. *Bull. Seism. Soc. Am.* **69**, 451–462.
- Hanks, T. C. (1981). Reply to W. Gawthrop’s comments on “The Lompoc, California earthquake (November 4, 1927; $M = 7.3$) and its aftershocks,” *Bull. Seism. Soc. Am.* **71**, 561–565.
- Hanks, T. C., J. A. Hileman, and W. Thatcher (1975). Seismic moments of the larger earthquakes of the Southern California region. *Geol. Soc. Am. Bull.* **86**, 1131–1139.
- Hanks, T. and A. C. Johnston (1992). Common features of the excitation and propagation of strong ground motion for North American earthquakes. *Bull. Seism. Soc. Am.* **82**, 1–23.
- Hanks, T. and H. Kanamori (1979). A moment magnitude scale. *J. Geophys. Res.* **84**, 2348–2350.
- Helmberger, D. V. and G. R. Engen (1980). Modeling the long period body waves from shallow earthquakes at regional distances. *Bull. Seism. Soc. Am.* **70**, 1699–1714.
- Hileman, J. A., C. R. Allen, and J. M. Nordquist (1973). Seismicity of the southern California region, 1 January 1931 to 31 December 1972, Seismological Laboratory, California Institute of Technology, 487 pp.
- Kanamori, H. (1978). Quantification of great earthquakes. *Tectonophysics* **49**, 207–212.
- Kanamori, H. (1988). Importance of historical seismograms for geophysical research, in *Historical Seismograms and Earthquakes of the World*, W. H. K. Lee (Editor) Academic Press, New York, 16–33.

- Kanamori, H. and K. Satake (1990). Broadband study of the 1989 Loma Prieta earthquake, *Geophys. Res. Lett.* **17**, 1179–1182.
- Liu, H. L. and D. V. Helmberger (1983). The near-source ground motion of the 6 August 1979 Coyote Lake, California, earthquake, *Bull. Seism. Soc. Am.* **73**, 201–218.
- McCulloch, D. S. (1987). Regional geology and hydrocarbon potential of offshore central California, in *Geology and Resource Potential of the Continental Margin of Western North America and Adjacent Ocean Basins, Beaufort Sea to Baja California*, vol. 6, D. W. Scholl, A. Grantz, and J. Vedder (Editors), American Association of Petroleum Geologists Circum. Pacific Earth Science, Houston, Texas, 353–401.
- Nicholson, C., C. Sorlien, and B. P. Luyendyk (1989). Reprocessing of Line RU-10, Offshore Southern Santa Maria Basin, California (abstract), *EOS* **70**, 1214–1215.
- Poppe, B. B. (1980). Directory of world seismograph stations. U.S. Geol. Surv. Report SE-25 on World Data Center A, James F. Landor, Director.
- Richter, C. F. (1958). *Elementary Seismology*, W. H. Freeman, San Francisco, 343 pp.
- Satake, K. and P. G. Somerville (1992). Location and size of the 1927 Lompoc, California earthquake from tsunami data, *Bull. Seism. Soc. Am.* **82**, 1710–1725.
- Somerville, P. G., J. P. McLaren, C. K. Saikia, and D. V. Helmberger (1990). The November 25, 1988 Saguenay, Quebec earthquake: source parameters and the attenuation of strong ground motion, *Bull. Seism. Soc. Am.* **80**, 1118–1143.
- Stewart, G. (1979). Summary of study of the November 4, 1927 Lompoc, California earthquake. Report to Pacific Gas and Electric Company.
- Wald, D. J., D. V. Helmberger, and S. H. Hartzell (1990). Rupture process of the 1987 Superstition Hills earthquake from the inversion of strong motion data, *Bull. Seism. Soc. Am.* **80**, 1079–1098.
- Wallace, T. C. and D. V. Helmberger (1982). Determining source parameters of moderate-size earthquakes from regional waveforms, *Phys. Earth. Planet. Interiors* **30**, 185–196.
- Woods, B. B., L. S. Zhao, D. V. Helmberger, H. K. Thio, and H. Kanamori (1992). The Loma Prieta earthquake sequence as observed at Pasadena (manuscript in preparation).
- Yeh, H. C. (1975). Mechanism of the 1927 Lompoc earthquake from surface waver analysis, *M.Sc. Thesis* University of Washington, Seattle.
- Zhao, L. S. and D. V. Helmberger (1991). Broadband modeling of the 25 November 1988, Saguenay earthquake at regional distances, *Geophys. J. Int.* **105**, 301–312.

CALIFORNIA INSTITUTE OF TECHNOLOGY
PASADENA, CALIFORNIA 91125
(DVH)

WOODWARD-CLYDE CONSULTANTS
566 EL DORADO STREET
PASADENA, CALIFORNIA 91101
(P.G.S., E.G.)

Manuscript received 12 July 1991